# Challenges and Advancements in Civil Engineering

K. Jagannadha Rao
Raghava Aditya B.
*Editors*

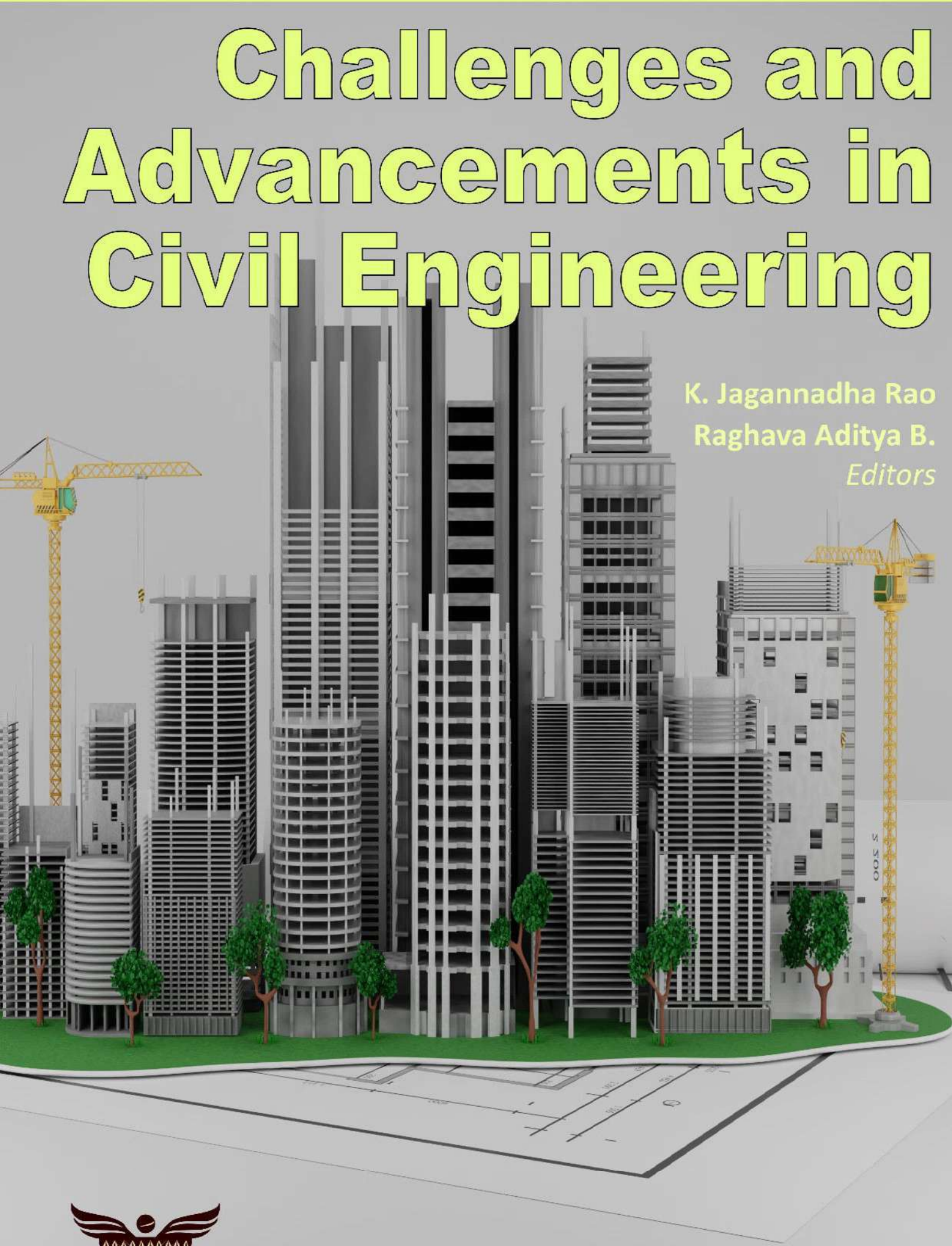

GRINREY PUBLISHING

In Book Series
Engineering Research Transcripts Volume 3 | 2023

Engineering Research Transcripts

Volume 03

# Challenges and Advancements in Civil Engineering

## Book Series by Grinrey Publications

- Research Transcripts in Energy
- Research Transcripts in Engineering
- Research Transcripts in Materials
- Research Transcripts in Computer, Electrical and Electronics Engineering


www.grinrey.com

Engineering Research Transcripts

Volume 03

# Challenges and Advancements in Civil Engineering

**K. Jagannadha Rao, Raghava Aditya B.**

Editors



Challenges and Advancements in Civil Engineering

K. Jagannadha Rao, Raghava Aditya B., editors (Chaitanya Bharathi Institute of Technology (A), Hyderabad, India)

Series: Engineering Research Transcripts

ISBN: 978-81-964105-0-6 (Ebook)

DOI: https://doi.org/10.55084/grinrey/ERT/978-81-964105-0-6

Published by: Grinrey Publishing

511, Ganesh Nakashtram, Dhayari, Pune, Maharashtra, India

www.grinrey.com

Email: contact@grinrey.com

# Contents


**Preface**

**1. Studies on the Performance of Under-reamed Piles in Sandy soil through Model Tests** **1**

*Ajai Joy Nariyelil, J Minu, Benny Mathews Abraham, Sobha Cyrus*

**2. Effect of Shape of Raft and Relative Density of Sand on Carrying Capacity of Model Piled Raft Foundation** **11**

*Arpita Vimlesh Patel, Nitin H Joshi*

**3. Assessment of Effect of Vehicular Emissions on Kanpur City Using Vulnerability Analysis** **25**

*Varun Yadav, Rajiv Ganguly*

**4. Compliance of Vehicular Emission Norms in Kanpur City, India** **33**

*Harshit Verma, Dipteek Parmar, Rajiv Ganguly*

**5. Dynamic Analysis of Multiple Fire Domino Effects for Better Environmental Safety and Health Management** **41**

*Anagha Raveendran, V R Renjith, G Madhu*

**6. Development of a Robotic Complex for the Manufacture of Parts Used in Civil Engineering** **51**

*Olga Afanaseva, Timur Tulyakov, Daniil Romashin, Anastasia Panova*

# Preface

**K. Jagannadha Rao, Raghava Aditya B.** (*Editors)*

Chaitanya Bharathi Institute of Technology (A), Hyderabad, India

Civil engineering is an important branch and always making human life safe and cheerfull. Researchers in the field of civil engineering are always enthusistaics and trying to overcome various challenges by providing advance solutions. The scope of civil engineering has widen considerably and it is demand of society to get better solutions through scientific research in various horisons of civil engineering. The better and durable structures, pleasant and healty environment, better transport and automation to assist consturction are some important topics included in this books thorugh six chapters.

First chapter describes an experimental study which is aimed to understand some factors affecting the under-reamed pile capacity in sand i.e. the bulb angle and bulb spacing. It also compares the variation of capacities of these piles in sand in both loose and dense state. The second chapter deals with the experimental study on an axially loaded model raft and piled raft foundation on sandy soil with square, circular, rectangular, and trapezoidal shapes of the raft.

Third chapter examined the effects of vehicular emissions on urban air quality and public health focusing on the impacts of the air pollution using a vulnerable analysis for Kanpur city, India. A study to determine the percentage of monitored automobiles in Kanpur, India, that abide by Bharat Stage-IV and VI (BS-IV and VI) emission criteria is presented in next chapter.

A quantitative analysis of the dynamic variation in time to failure and failure probabilities of storage tanks during multiple fire domino effects is presented in chapter five. The concept of critical thermal dose is applied in this study for the estimation of dynamic time to failure of each vulnerable storage tank considering maximum synergistic effects based on the temporal variation in the intensity of heat radiation received by them.

The last article proposes a methodology for the development of a robotic complex for the manufacture of building parts. An analysis was carried out to select the most preferable option for the layout of the robotic complex and the option was selected using the method of the resulting quality indicator, consisting of an industrial floor robot, a mechatronic lathe and a storage device.

We believe the articles published in this book will be useful for future researchers and students as references in the respective fileds.

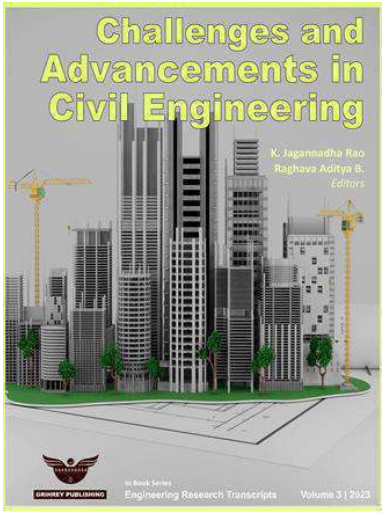


Online: 28 Sep 2023

DOI: https://doi.org/10.55084/grinrey/ERT/978-81-964105-0-6

1

# Studies on the Performance of Under-reamed Piles in Sandy Soil through Model Tests

**Ajai Joy Nariyelil [a,*], J Minu[a], Benny Mathews Abraham[a,b], Sobha Cyrus[a]**

[a] School of Engineering, Cochin University of Science and Technology, Kochi, India

[b] Albertian Institute of Science and Technology, Kochi, India

*ajaijoynariyelil@gmail.com

## Abstract

Predicting pile behavior and estimating pile capacity in different soil conditions are critical in building industry. This paper describes an experimental study which is aimed to comprehend some factors affecting the under-reamed pile capacity in sand i.e. the bulb angle and bulb spacing. It also compares the variation of capacities of these piles in sand in both loose and dense state. A total of 9 model piles were tested, which included four single under-reamed piles, four double under-reamed piles and a normal pile. From the experimental studies, load–settlement curves are obtained and the pile capacities are determined using various criteria reported in the literatures. The capacity increased to at least twice the value when an under-ream bulb was introduced to a normal pile. The pile with bulb angle of $45^0$ and with bulb spacing of 1.25 times the bulb diameter showed maximum capacity for single under-reamed and double under-reamed piles, respectively. The pile capacity increased with increase in sand density. The test results are in agreement with the relevant Indian Standards.

**Keywords**

Bulb angle, Bulb spacing, Under-reamed piles

Received: 04 Apr 2023 | Accepted: 30 Aug 2023 | Online: 28 Sep 2023

**Cite this article**

Ajai Joy Nariyelil, J Minu, Benny Mathews Abraham and Sobha Cyrus (2023). Studies on the Performance of Under-reamed Piles in Sandy soil through Model Tests. *Engineering Research Transcripts*, 3, 1–9.

DOI: https://doi.org/10.55084/grinrey/ERT/978-81-964105-0-6_1

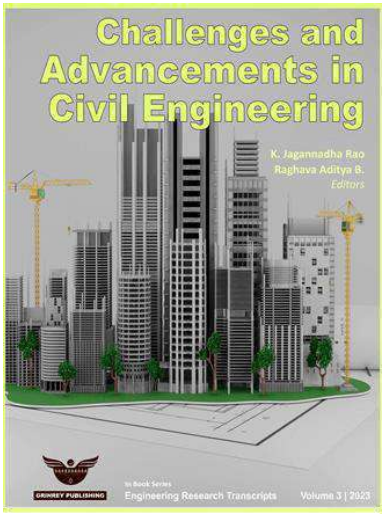

## 1. Introduction

Pile foundations are frequently used to effectively transmit load from the superstructure to greater depths if some weak strata overlie a firm stratum. Under-reamed pile foundations are those among such deep foundations which are used when the subsurface soil has inadequate strength. They can be either bored compaction piles or cast in place piles. The 1940s saw the introduction to the practice of employing under-reamed piles and since the 1950s, they have been widely used in India, where there was a lot of expansive black cotton soil.

Under-reamed piles are cast-in-place concrete piles having one or more under-ream bulbs along their stems, which enhances pile capacity under compression and tension loads [1]. These piles can lessen the impact of negative skin friction and enhance tip resistance and pile shaft friction [2]. Under-reamed piles which have projections known as bulbs or under-reams which increases its load-carrying capacity under compression, tension, and lateral loading [3-12]. Nazir et al. [13] concluded that the ultimate load could be worked out using time-settlement plot from the pile load test results. According to results of the studies by Harris et al. [14], the uplift capacity declined as the angle of the under-reams increased. The safe pile capacity as determined by subsoil parameters differs from that specified in the IS 2911- Part 3 [15], according to a research done on multiple under-reamed piles of variable diameter and length at various sites by Pakrashi [16]. The results of a numerical study by Jebur et al. [17] on the geometrical form of bulbs revealed that the ream's cone shape is preferred over other under-reamed bulb shapes in terms of reducing vertical displacement. These reams, according to Jebur and Ahmed [18], improve both friction and bearing surface, as well as pile capacity in compressive stress. Therefore, these type of piles are successfully employed for machine foundations and electrical transmission tower foundations. The capacity of the piles in compression and tension was significantly impacted by the number, size, shape, and position of the bulbs [19]. Various studies were also conducted to understand the influence of geometrical features of the under-reamed pile on its ultimate capacity by Christopher and Gopinath [20], Shetty et al. [21] and Shrivastava and Bhatia [22].

Bulbs are regarded as the most significant advantage of under-reamed piles over other types of piles because appropriate performance may be attained with smaller stem diameters and lengths. They can be utilized instead of long and broad piles for bearing heavy loads. This implies that the economic properties of under-reamed piles are also taken into account throughout the design process. This study examined the efficiency of the single and double under-reamed pile installed in loose and dense sand and compared the results with that of a normal pile. Single under-reamed piles of various under-ream angles and double under-reamed piles with different under-ream spacings were analyzed and the most efficient one was found out. The study also compared the variation in capacity of piles at different sand density.

## 2. Materials

### 2.1. Soil

The accessible local river sand is used for the model test. Laboratory investigations are done to find out the basic soil parameters of river sand. The tank is filled with particles that passed through an IS sieve with size of 4.75mm. Model tests are carried out on both dense and loose sand. Table 1 summarizes the basic properties of the sand.

### 2.2. Under-reamed Pile Models

Timber (Mahogany) was used to construct the pile models. A total of 9 distinct pile models were made, each having a length of 450 mm and stem diameter of 40 mm. The bulb diameter ($D_u$) of the under-reamed piles were taken as 100 mm which was 2.5 times the stem diameter. Four piles were single under-reamed piles with various bulb angles of $15^0$, $30^0$, $45^0$, and $60^0$. Then, there were four double under-reamed piles

with different bulb spacings: $1.0D_u$, $1.25D_u$, $1.5D_u$, and $1.75D_u$ with a constant bulb angle of $45^0$. And the final pile created was a normal pile with no bulbs or projections. The images of the pile models used in the study are given in Figure 1 and 2.

**Table 1.** Properties of Sand

| **Properties** | | **Capacity** |
|---|---|---|
| Dry Unit Weight (kN/m$^3$) | Loose Sand | 13.9 |
| | Dense Sand | 16 |
| Angle of Internal Friction (degrees) | Loose Sand | 28 |
| | Dense Sand | 37 |
| Uniformity Coefficient | | 2.86 |
| Fineness Modulus | | 3 |
| Particle Size Distribution (%) | Gravel Size (4.75 mm – 80 mm) | 0 |
| | Sand Size (0.075 mm -4.75 mm) | 100 |
| | Silt Size (0.002 mm - 0.075 mm) | 0 |

**Fig. 1.** Models of normal and single under-reamed piles.

**Fig. 2.** Models of double under-reamed piles.

### 2.3. Metal Tank

The pile model tests were conducted in a metal tank with measurements of 450 mm x 450 mm x 600 mm whose size was set based on the pile diameter. Boundary effects were thought to be insignificant considering the size of the tank.

## 3. Methodology

### 3.1. Filling the Tank

In loose state, a pouring device filled with sand wass moved spirally from outside towards centre, while maintaining a height of fall of 250 mm. The model pile for testing was positioned vertically and lined up with the loading mechanism after the tank's bottom 150 mm of space had been filled. The remaining portion of the tank was filled similarly without disturbing the model pile. For sand in dense state, the depth of the tank was divided into layers of 50 mm. Sand was filled in layers, and each layer was thoroughly tamped

with a cylindrical weight (30 N). To achieve adequate compaction of the sand layers, each layer received around 60 strikes from the weight. The appropriate model pile was installed after filling the bottom 150 mm (3 layers), and the remaining tank was filled using the same method without moving the model pile. Once the tank was filled, the top surface was levelled, and the experimental setup was established.

### 3.2. Loading Mechanism

A hydraulic loading mechanism was used for this study. By pumping oil, load was applied, and a proving ring with a capacity of 10 kN was used to measure the load. The tank was placed on the loading frame and load was applied using a hydraulic jack. Figure 3 shows the test setup used for the study.

### 3.3. Test Procedure

Based on the procedures described in the preceding section, the metal tank was filled with sand. Using a hydraulic jack, an external compressive load was applied gradually. Such manually controlled hydraulic jack has been employed for compressive loading in past studies [23]. A proving ring connected to the test setup was used to measure the external load that has been imposed. To measure the settlement, two dial gauges were employed. Load was applied until the displacement exceeded 12 mm or the proving ring began to produce a steady reading with continuous settling. Finally, the ultimate capacities corresponding to 12 mm, 7.5 mm (7.5% of $D_u$), and 4 mm (10% of D) settlements were calculated using the load-settlement curves plotted from the recorded data.

**Fig. 3.** Test Setup

## 4. Results and Discussions

### 4.1. Tests in Loose Sand

#### 4.1.1 Single Under-reamed Pile

From figure 4, it can be seen that for varying bulb angles, the capacity is maximum for the pile with $45^0$ bulb angle. Single under-reamed pile with bulb angle $45^0$ has clearly the maximum ultimate capacity corresponding to all the settlements considered and the minimum capacity was obtained for the pile with $60^0$ bulb angle. The introduction of under-reams increased the capacity significantly and for the pile with $45^0$ bulb angle, the capacity increased to nearly 4.5 times the capacity of normal pile for 12 mm settlement. The maximum capacity observed for $45^0$ bulb angle agrees with the suggestions of IS 2911- Part 3: 1980 [15].

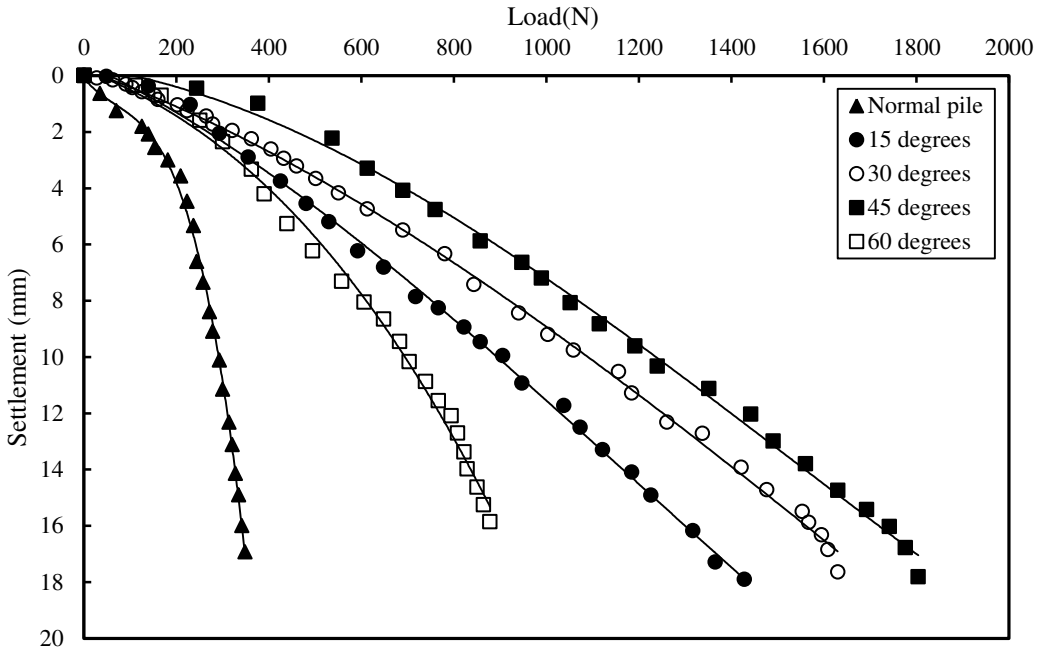


**Fig. 4.** Load-settlement curves for single under-reamed piles tested in loose sand.

### 4.1.2 Double Under-reamed Pile

From the load settlement curves as shown in figure 5, it can be seen that the double under-reamed pile with an under-ream spacing of $1.25D_u$ has a slightly higher capacity as compared to others. The capacity of pile with bulb spacing $1.5D_u$ is comparable to that of the pile with $1.25D_u$ bulb spacing at 12 mm settlement and the pile with $1.0D_u$ bulb spacing has the least capacity as compared to all other double under-reamed piles. Also, it should be noted that the capacity of the pile with $1.25D_u$ bulb spacing is nearly 7 times higher in comparison with a normal uniform diameter pile and nearly 1.5 times higher in comparison with single under-reamed pile with $45^0$ bulb angle. These maximum capacity observed for $1.25D_u$ bulb spacing is in agreement with the suggestions given by IS 2911 – Part 3: 1980 [15].

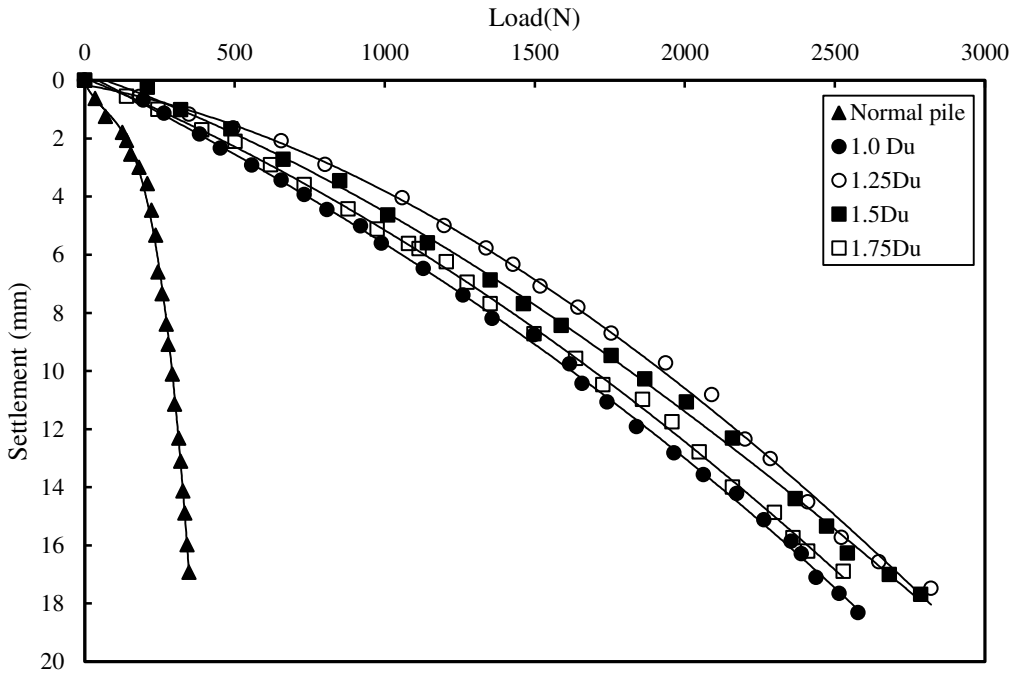


**Fig. 5.** Load-settlement curves for double under-reamed piles tested in loose sand.

### 4.2. Tests in Dense Sand

#### 4.2.1 Single Under-reamed Pile

The load settlement plots, as in figure 6, show that under-reamed pile with bulb angle of $45^0$ clearly has the maximum capacity corresponding to all the settlements considered. Minimum capacity was obtained for the pile with $60^0$ bulb angle. The introduction of under-reams increased the capacity significantly and for the pile with $45^0$ bulb angle the capacity increased to nearly 4 times the capacity of normal pile for 12 mm settlement. So, ,it is quite evident that the trends are similar to that in loose sand. Also, the results agree with the suggestions in IS 2911- Part 3: 1980 [15] for providing an under-ream angle of $45^0$.

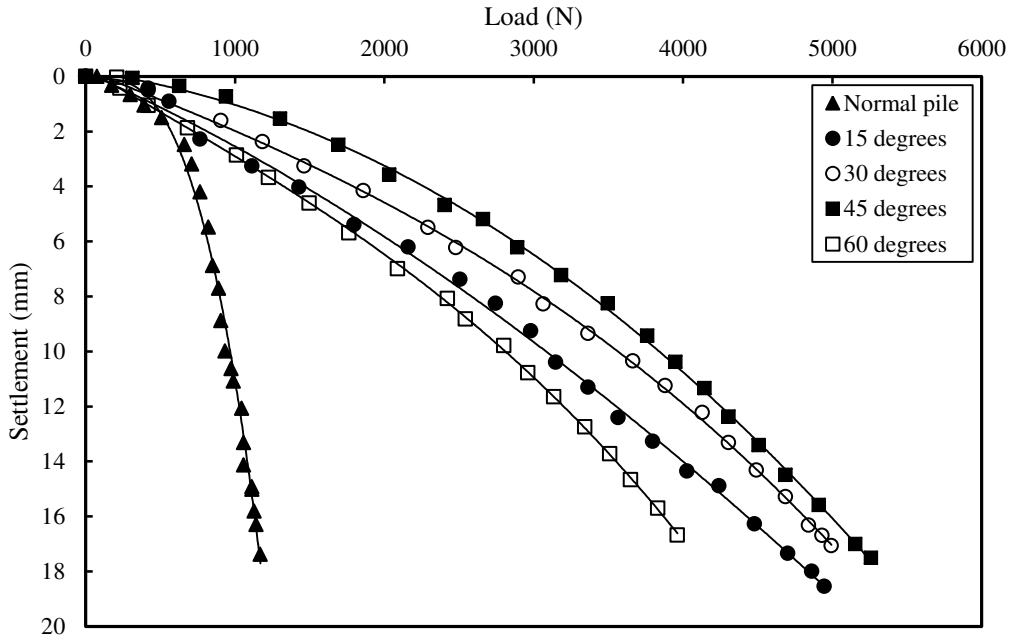


**Fig. 6.** Load-settlement curves for single under-reamed piles tested in dense sand.

#### 4.2.2 Double Under-reamed Pile

From the load-settlement plot shown in figure 7, it can be inferred that the capacity of double under-reamed pile with bulb spacing $1.0D_u$ has the least capacity. Corresponding to all the three settlements considered, the ultimate capacity of double under-reamed pile with bulb spacing $1.25D_u$ has the maximum value, which is in agreement with the suggestion by IS 2911- Part 3. Another important observation is, that the capacity of the pile with $1.25D_u$ bulb spacing is nearly 7 times higher in comparison with a normal uniform diameter pile and nearly 1.5 times higher in comparison with single under-reamed pile with $45^0$ bulb angle.

### 4.3. Variation in Capacity with Density of Sand and Number of Bulbs

In this study the tests were conducted in two densities of sand. Table 2 shows the capacities of normal piles, single under-reamed piles (with $45^0$ bulb angle) and double under-reamed piles (with $1.25D_u$ bulb spacing and $45^0$ bulb angle) in both these densities i.e. loose state and dense state. From this data it is evident that, as the density of sand increases the capacity of the pile also increases. Here, for the change in density from 13.9 to 16 kN/m$^3$, the capacity of the all the piles, i.e. normal, single under-reamed and double under-reamed piles, increased to almost 3 times. This is due to the higher angle of internal friction which increases the surface interaction between the pile and sand. Also, from the table 2 it is evident that as the number of bulbs increased the capacity of piles increased by quite a margin, as we have discussed in the preceding sections.

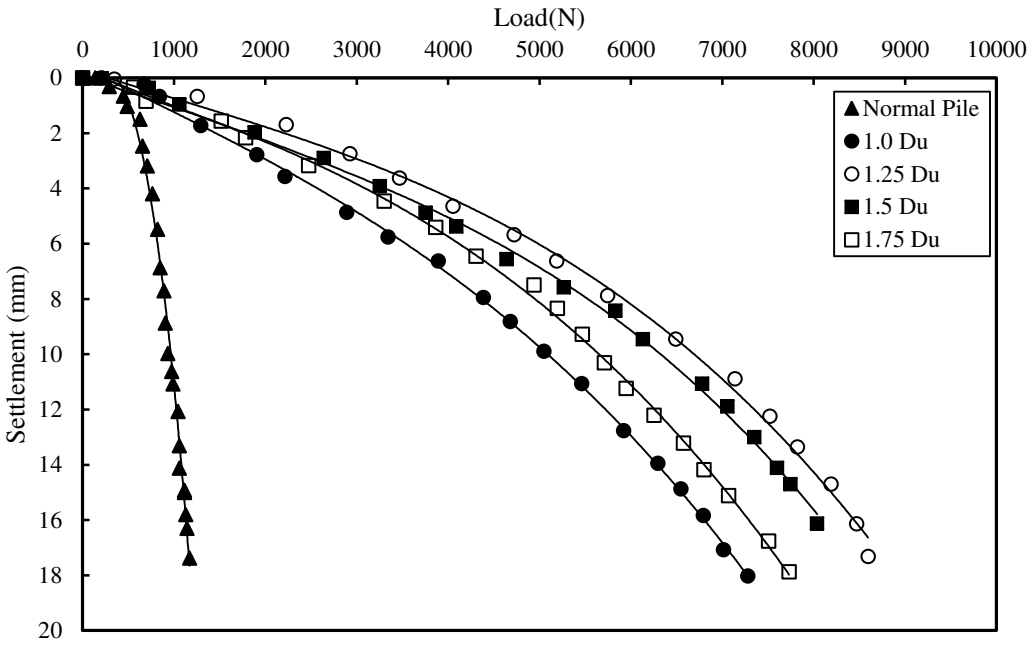


**Fig. 7.** Load-settlement curves for double under-reamed piles tested in dense sand.

**Table 2.** Capacities of Piles corresponding to12 mm settlement in different densities of sand

| Material | Capacity (N) | |
|---|---|---|
| | Loose Sand | Dense Sand |
| Normal Pile | 310 | 1000 |
| Single Under-reamed Pile | 1450 | 4210 |
| Double Under-reamed Pile | 2220 | 7390 |

## 5. Conclusions

The current study attempted to understand various parameters that influence the capacity of under-reamed piles, such as bulb angle, bulb spacing, number of bulbs and sand density. A series of model tests revealed that the capacity of under-reamed piles is actually controlled by the aforementioned criteria. In conclusion, the introduction of an under-ream bulb significantly enhances the load-bearing capacity of normal uniform diameter piles, with capacity increasing by at least twice the original value. This study confirms the prevailing practice of using a $45^0$ bulb angle for under-reamed piles, both single and double, which yielded the highest capacity. Furthermore, the optimal configuration for double under-reamed piles involves a bulb spacing of $1.25D_u$ and a bulb angle of $45^0$. The study demonstrated that increasing the number of bulbs from one to two further enhances capacity, regardless of the sand density. Notably, the findings align with the recommendations outlined in IS 2911 - Part 3: 2010, supporting the practical application of a $45^0$ bulb angle and advocating for bulb spacing between $1.25D_u$ and $1.5D_u$ for double under-reamed piles in sandy soil. This comprehensive investigation contributes valuable insights to the field of foundation engineering and reinforces the soundness of existing design guidelines for optimizing the load-bearing performance of under-reamed piles in various sandy soil.

## Nomenclature

$D$ : Stem Diameter

$D_u$ : Bulb Diameter

## References


[1] Farokhi, A. S., Alielahi, H., and Mardani, Z. (2014). Optimizing the performance of under-reamed piles in clay using numerical method. Electronic Journal of Geotechnical Engineering, 19(Bundle G), 1507-1520.

[2] Chandrasekaran, V., Garg, K. G., and Prakash, C. (1978). Behaviour of isolated bored enlarged base pile under sustained vertical loads. Soils and Foundations, 18(2), 1-15.

[3] Cooke, R. W., and Whitaker, T. (1961). Experiments on model piles with enlarged bases. Geotechnique 11 (1), 1–13.

[4] Prakash, C., and Ramakrishna, V.V.G.S.T. (2004). Lateral load capacity of underreamed piles: an analytical approach. Soils Found. 44 (5), 51–65.

[5] Peter, J. A., Lakshmanan, N., and Manoharan, P. D. (2006). Investigations on the static behavior of self-compacting concrete under-reamed piles. J. Mater. Civ. Eng. 18 (3), 408–414.

[6] Khatri, V. N., Kumar, A., Gupta, S. K., Dutta, R. K., and Gnananandarao, T. (2019). Numerical study on the uplift capacity of under-reamed piles in clay with linearly increasing cohesion. Int. J. Geotech. Eng. 1–12. https://doi.org/10.1080/ 19386362.2019.1660527.

[7] Kumar, A., Khatri, V. N., and Gupta, S. K. (2020). Effect of linearly increasing cohesion on the compression and uplift capacity of the under-reamed pile in clay. SN Appl. Sci. 2 (2), 1–17.

[8] Kumar, A., Khatri, V. N., and Gupta, S. K. (2021). Numerical and analytical study on uplift capacity of under-reamed piles in sand. Mar. Georesour. Geotechnol. 1–38. https:// doi.org/10.1080/1064119X.2021.1871689.

[9] Majumder, M., and Chakraborty, D. (2021). Three-dimensional numerical analysis of under-reamed pile in clay under lateral loading. Innovative Infrastructure Solutions 6 (2), 1–17.

[10] Majumder, M., and Chakraborty, D. (2021). Bearing and uplift capacities of under-reamed piles in soft clay underlaid by stiff clay using lower-bound finite element limit analysis. Front. Struct. Civ. Eng. 15 (2), 537–551.

[11] Majumder, M., and Chakraborty, D. (2021). Effects of scour-hole depth on the bearing and uplift capacities of under-reamed pile in clay. Ocean Eng. 240, 109927.

[12] Majumder, M., and Chakraborty, D. (2021). Effects of scour-hole dimensions and bulb positions on the lateral response of under-reamed pile in soft clay. Appl. Ocean Res. 117, 102942.

[13] Nazir, R., Moayedi, H., Mosallanezhad, M., and Tourtiz, A. (2015). Appraisal of reliable skin friction variation in a bored pile. Proceedings of the Institution of Civil Engineers-Geotechnical Engineering, 168(1), 75-86.

[14] Harris, D. E., and Madabhushi, G. S. P. (2015). Uplift capacity of an under-reamed pile foundation. Proceedings of the Institution of Civil Engineers-Geotechnical Engineering, 168(6), 526-538. https://doi.org/10.1680/jgeen.14.00154

[15] IS: 2911 Part III. (1980). Code of Practice for Design and Construction of Pile Foundations: Underreamed Piles. New Delhi, India: Bureau of Indian Standard.

[16] Pakrashi, S. (2017). A Comparative Study on Safe Pile Capacity as Shown in Table 1 of IS 2911 (Part III): 1980. Journal of The Institution of Engineers (India): Series A, 98(1), 185-199.

[17] Jebur, M. M., Ahmed, M. D., and Karkush, M. O. (2020). Numerical analysis of under-reamed pile subjected to dynamic loading in sandy soil. In IOP conference series: materials science and engineering (Vol. 671, No. 1, p. 012084). IOP Publishing.

[18] Jebur, M. M., and Ahmed, M. D. (2020). Experimental investigation of under reamed pile subjected to dynamic loading in Sandy soil. In IOP conference series: materials science and engineering (Vol. 901, No. 1, p. 012003). IOP Publishing.

[19] Kurian, N. P., and Srilakshmi, G. (2010). Studies on the geometrical features of under-reamed piles by the finite element method. Journal of Karunya University, 2(1), 1-14.

[20] Christopher, T., and Gopinath, M. B. (2016). Parametric study of under-reamed piles in sand. International Journal of Engineering Research & Technology (IJERT), 5(7), 577-581.

[21] Shetty, P., Naveen, B. S., and Kumar, N. B. S. (2015). Analytical study on geometrical of underreamed pile by Ansys. International Journal of Modern Chemistry and Applied Science, 2(3), 174-180.

[22] Shrivastava, N., and Bhatia, N. (2008). Ultimate bearing capacity of under-reamed pile-finite element approach. In The 12th International Conference of International Association for Computer Methods and Advances in Geomechanics (IACMAG) (pp.1-6).

[23] Hegde, A., and Sitharam, T. G. (2015). Experimental and analytical studies on soft clay beds reinforced with bamboo cells and geocells. International Journal of Geosynthetics and Ground Engineering, 1, 1-11.

2

# Effect of Shape of Raft and Relative Density of Sand on Carrying Capacity of Model Piled Raft Foundation

**Arpita Vimlesh Patel*, Nitin H Joshi**

Applied Mechanics Department, Faculty of Technology & Engineering, The M S University of Baroda, India

*arpsoham@gmail.com

## Abstract

A pile-raft foundation proves to be an economical foundation in many situations as compared to a pile foundation, but its analysis is complicated because of interactions between the pile, the raft, and the soil. This research paper presents the experimental study on an axially loaded model raft and piled raft foundation on sandy soil with different shapes of the raft (square, circular, rectangular, and trapezoidal). The study was carried out by varying the relative density of the sand bed (40%, 60%, and 80%). The spacing between piles was kept 7d for all model piled-raft foundations (MPRF). Initial Yield Load (IYL) and Final Yield Load (FYL) of MPRF were calculated as per the Poulos-Davis-Randolph (PDR) philosophy. It was observed that as the relative density of sand increases, the IYL and FYL of piled raft foundations of all shapes increase. The IYL and FYL were observed to increase with an increase in the relative density of sand in the MPRF for all shapes of raft. The higher IYL and FYL were observed mostly in MPRF with a square raft.

**Keywords**

Final Yield Load; Initial Yield Load; model piled raft foundation

Received: 25 Mar 2023 | Accepted: 05 Sep 2023 | Online: 28 Sep 2023

**Cite this article**

Arpita Vimlesh Patel and Nitin H Joshi (2023). Effect of Shape of Raft and Relative Density of Sand on Carrying Capacity of Model Piled Raft Foundation, *Engineering Research Transcripts*, 3, 11-24.

DOI: https://doi.org/10.55084/grinrey/ERT/978-81-964105-0-6_2

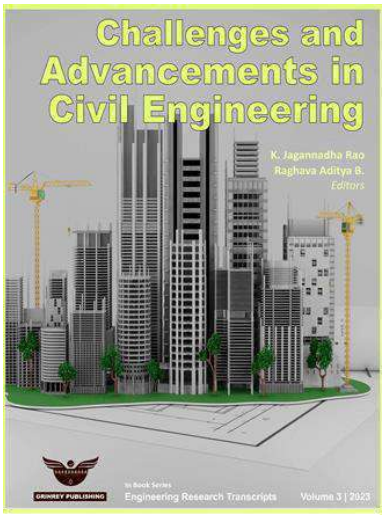

## 1. Introduction

Piled raft foundations have been developed and are commonly used to support superstructures such as high-rise buildings, bridges, power plants, and other civil structures, as well as to prevent excessive settlements. The design of such foundations, however, has become complicated due to the load-sharing mechanism of the pile-raft-soil system. When compared to traditional pile foundations, where only piles are used to reduce total and differential settlements and the raft's contribution is generally ignored, the piled raft foundation method has been shown to be a cost-effective foundation type [7].

There are several studies found in the literature that focused on parameters such as the number of piles, length of piles, diameter of piles, pile spacing, positioning of piles, stiffness of piles, load distribution, load level, raft thickness, raft dimensions [1] [2] [3] [4] [5], and type of soil, but the shape of the raft with an equal contact area was missing. The goal of this research was to evaluate the performance of a model piled raft foundation lying on a sand bed with varying relative density and raft shapes with equal contact area.

## 2. Materials and methods

In this research work, laboratory model tests were conducted on unpiled raft and piled rafts with different shapes of raft supported on loose to dense sand conditions (RD = 40%, 60%, and 80%). The laboratory model tests were carried out on model rafts made up of mild steel plates with sizes of 220mm × 220mm × 25mm thick (Square Shape), 248.24mm diameter × 25mm thick (Circular Shape), 260mm ×186.1mm × 25mm thick (Rectangular Shape), 240mm (long side) × 230mm (cross side) ×180mm (short side) × 25mm thick (Trapezoidal Shape) .The contact area of all raft shapes was kept constant. In the laboratory test, model mild steel piles with hollow circular cross sections and 9.7mm external diameter, 0.95mm thickness, and a length of 291mm were used to represent the length to external diameter (l/d) ratio of 30. The bottom of the pile was kept in a closed cone with a 120° angle of cone. The piled raft was used, which consisted of a group of piles in a square pattern arrangement of 3x3 groups (9 piles) with 7d spacing located centrally screwed below the raft. To this end, an experimental setup was created to imitate the piled-raft foundation using various parameters. These are discussed in the following section:

### 2.1 Material Properties

#### 2.1.1 Sand

Commercially available Orsang river sand was used as a foundation soil. Fig. 1 depicts the particle size distribution curve of Orsang river sand. The index properties and shear strength properties of sand are listed in Table 1.

#### 2.1.2. Model pile

Mild steel rods with a hollow circular cross section having a 9.7mm external diameter, 0.95mm thickness, and length to external diameter (L/d) ratio of 30 were used as model piles (Fig. 2). The bottom part of the pile was a closed cone with a 120° angle. Threads were provided at the top end of the inner side of the piles to fix them to the raft using a screw from the top of the raft, generating monolithic action between the piles and the raft.

**Fig. 1.** Model pile

### 2.1.3 Model Raft

Mild steel plates were used to prepare the rigid model rafts. The dimensions of model rafts with different shapes are as shown in Table 2. Fig. 3 shows the detailed dimensions of a model raft with the arrangement of earth pressure cells (EPC) and piles. Small circle having 10mm diameter and big circle having 31mm diameter in Fig. 2 display the position of piles and EPC in MPRF respectively.

### 2.1.3 Model Piled Raft

The model piled raft was prepared by fixing the pile group below the raft. The pile group consisted of nine piles in a square pattern with centre-to-centre spacing between the piles 7d. The pile group was secured beneath the raft in such a way that the raft's centre of gravity and the pile group's centre of gravity coincided.

**Table 1.** Index properties and shear strength properties of sand

| Sr. No. | Property | Unit | Values |
|---|---|---|---|
| 1 | Specific Gravity | - | 2.55 |
| 2 | Particle Size Distribution | | |
| | Gravel (greater than 4.75mm size) | Percentage | 2.08% |
| | Coarse Sand (4.75 mm – 2mm) | Percentage | 2.2% |
| | Medium sand (2mm – 0.425mm) | Percentage | 63.5% |
| | Fine Sand (0.425mm – 0.075mm) | Percentage | 30.9% |
| | Silt (less than 0.075mm) | Percentage | 1.3% |
| 3 | $D_{10}$ | mm | 0.25 |
| 4 | $D_{30}$ | mm | 0.41 |
| 5 | $D_{60}$ | mm | 0.70 |
| 7 | Coefficient of Uniformity (Cu) | - | 2.75 |
| 8 | Coefficient of Curvature (Cc) | - | 0.95 |
| 9 | Type of sand as per IS code method (sieve analysis) | - | SP |
| 10 | Maximum unit weight | ($kN/m^3$) | 18.3 |
| 11 | Minimum unit weight | ($kN/m^3$) | 15 |
| 12 | Unit weight of sand at 40% Relative Density (RD) | ($kN/m^3$) | 16.2 |
| 13 | Unit weight of sand at 60% Relative Density (RD) | ($kN/m^3$) | 16.8 |
| 14 | Unit weight of sand at 80% Relative Density (RD) | ($kN/m^3$) | 17.5 |
| 15 | Angle of internal friction at 40% RD | degree | 32 |
| 16 | Angle of internal friction at 60% RD | degree | 35 |
| 17 | Angle of internal friction at 80% RD | degree | 39 |

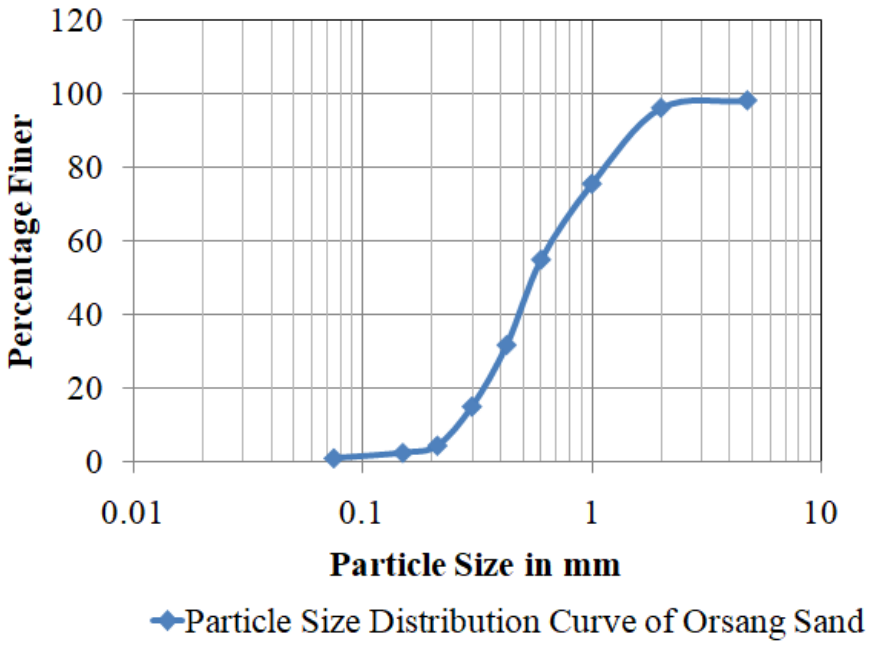


**Fig. 2.** Particle size distribution curve of the Orsang river sand (Sieve Analysis Test)

**Table 2.** Dimensions of different shape of model raft

| Shape of model raft | Plan dimensions of model raft (mm) | Plan area of raft ($mm^2$) | Thickness of model raft (mm) |
|---|---|---|---|
| Square | 220 x 220 | 48400 | 25 |
| Circular | 248.24 (Dia.) | 48400 | 25 |
| Rectangular | 260 x 186.15 | 48400 | 25 |
| Trapezoidal | Long side- 240<br>Short side- 180<br>Cross size- 230 | 48400 | 25 |

## 2.2 Experimentation

### 2.2.1 Experimental Set up

The model tests were performed in a tank that measured 1200 mm×1200 mm in plan and 1070 mm in depth and was made of mild steel plate, one-sided Perspex sheet, and angle stiffeners. The tank was supported by a reaction loading frame constructed of channel and angle sections. The mechanical screw jack was attached centrally on the top of the reaction frame, as shown in Fig. 4 and 5. A proving ring was held between the raft and the mechanical screw jack to measure the load. Four linear displacement transducers (LVDTs) with 0.01 mm accuracy were placed at the raft's corners to measure vertical settlement. Averaging the LVDT readings yielded the average settlement. Earth pressure cells (EPC) were placed in the groves at the bottom of the raft in such a way that the bottom surface of the raft and the EPC met in a plane, as shown in Fig. 3, to investigate the contact pressure distribution between the raft and the soil. The earth pressure cells were 30mm in diameter and 12mm in thickness.

### 2.2.2 Testing Procedure:

The test procedure consisted of the following steps:

1. The tank's total height was divided into 50 mm intervals. The sand was filled in the tank in layers and vibrated with a surface vibrator for a specific time to achieve the desired relative density, the details of which are given in Table 3. The dimensions, weight, and frequency of the surface vibrator used are 320mm x 310mm, 16.9 kg, and 1400 rpm, respectively. The tank was filled up to a height of 800 mm with sand.
2. The sand was filled in layers in the tank until it reached 55 cm / 60cm thickness, at which point the combined model of the pied raft was kept such that the center of gravity of the raft aligned with the center of the mechanical screw jack using a plumb bob and spirit level for leveling on the sand bed. It was driven 5cm into the sand bed from its previous position by pressing it with the mechanical screw jack. The sand at the periphery of the raft was vibrated with a vibrator. For compaction in the central portion of the piled raft, the raft was removed from the top by unscrewing, and sand between the piles was compacted using a narrow, 10 mm-thick, 58mm-wide mild steel plate by tamping. The tank was filled up to 800 mm with the required relative density of sand, and the raft was reconnected with the piles such that it flushes with the surface of the sand bed. The density of the sand was checked by placing strong wooden boxes of 15 cm × 10cm × 7.5cm at different elevations within the tank.
3. The proving ring for measuring load on the raft/piled raft was placed in the center of the model, so that it coincided with the center of the mechanical screw jack. A small metal ball was kept between the proving ring and the mechanical screw jack so that the model could be subjected to concentric load. To calculate the settlement due to the applied load, four LVDTs with a sensitivity of 0.01 mm were placed at the four corners of the raft.
4. The maintained load test (MLT) method was used for all tests, and the load increment was kept at 1/10th of the estimated ultimate capacity of an unpiled or piled raft, as the case may be. The load increment was held until the rate of settlement became negligible (0.01 mm per 5 minutes). The procedure was repeated until the large progressive settlement was reached or failure was noticed.
5. When the readings were stabilized, the settlement and EPC readings were taken for each load increment.

**Table 3.** Details of parameters used to achieve the desired density of sand using surface vibration technique

| Sr.No. | Unit Weight ($kN/m^3$) | Relative Density (RD) (%) | Thickness of Layer (mm) | Mass of sand filled in each layer (kg) | Duration of Vibration (sec) |
|---|---|---|---|---|---|
| 1 | 16.2 | 40 | 150 | 349.92 | 45 |
| 2 | 16.8 | 60 | 100 | 241.92 | 85 |
| 3 | 17.5 | 80 | 50 | 126 | 60 |

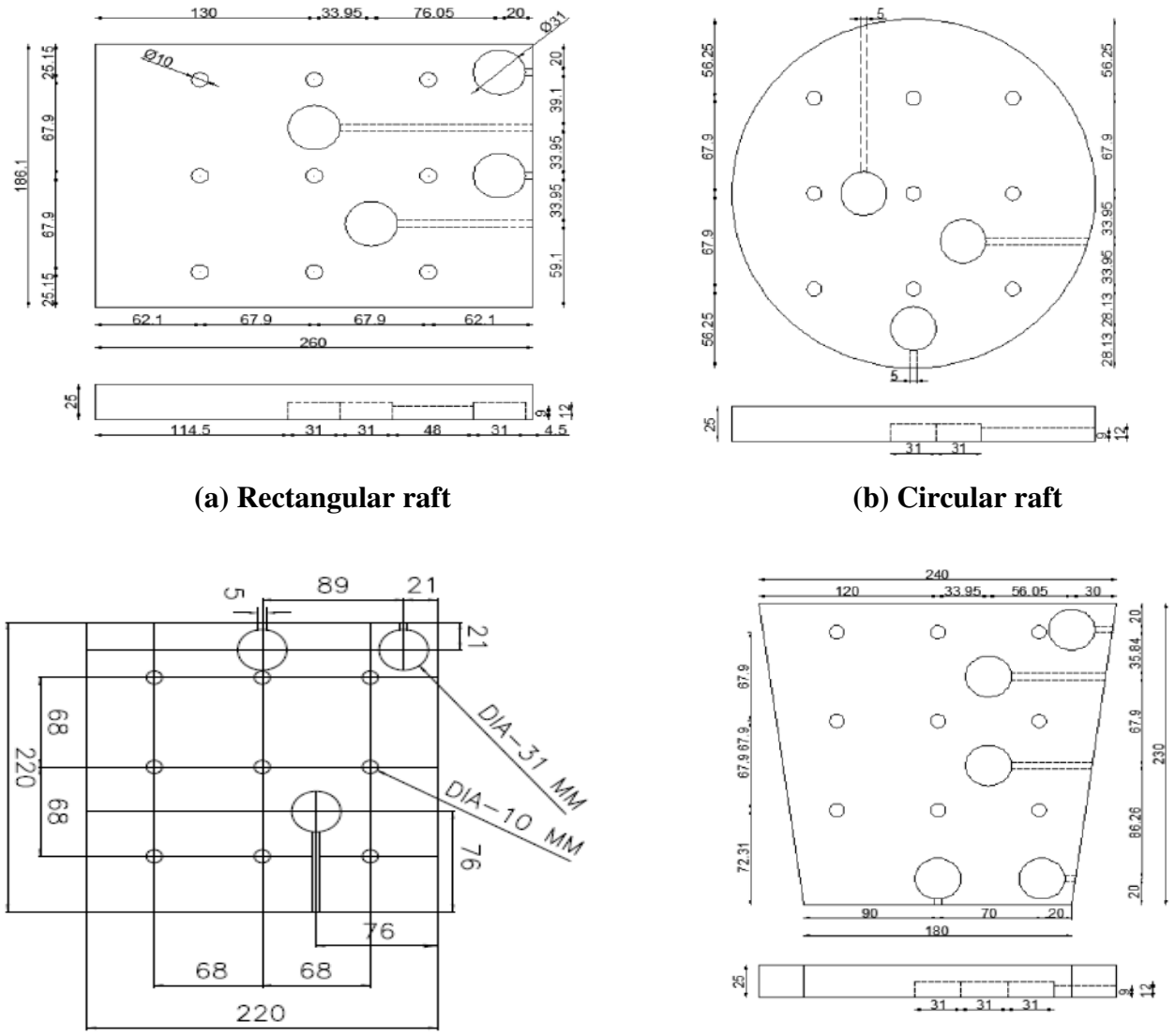


**Fig. 3.** Detailed dimensions of model raft

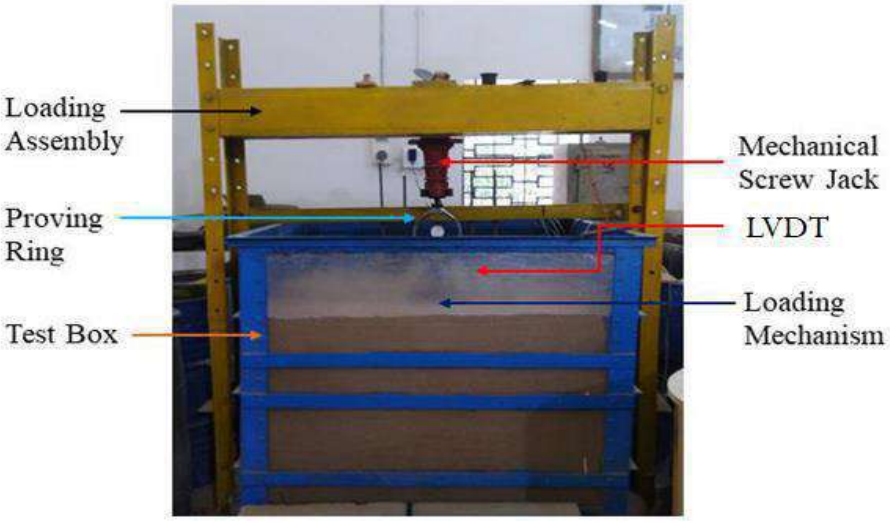


**Fig. 4.** Experimental Set up

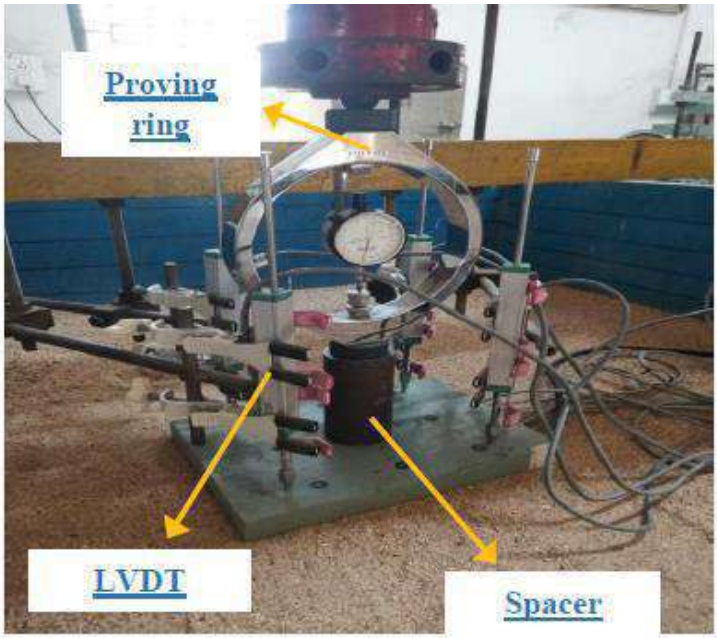


**Fig. 5.** Loading setup detail

## 3. Results and Discussion

### 3.1 Load settlement curve

The results obtained from experiments are analyzed as follows:

The analysis of unpiled raft (UR) was carried out as per the intersection tangent method, and the load settlement curve of a piled raft foundation was analysed as per the Poulos-Davis-Randolph (1980) Approach (tri-linear behaviour) generally known as the PDR method for piled raft foundation, as shown in Fig. 6 and 7, respectively.

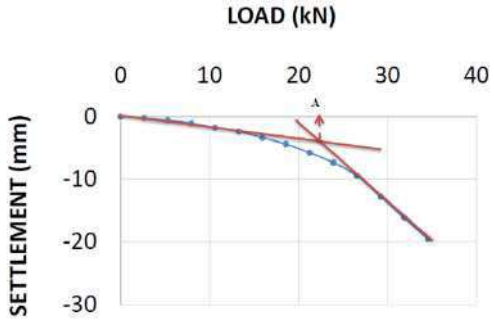


**Fig. 6.** Ultimate load of un-piled raft as per intersection tangent method

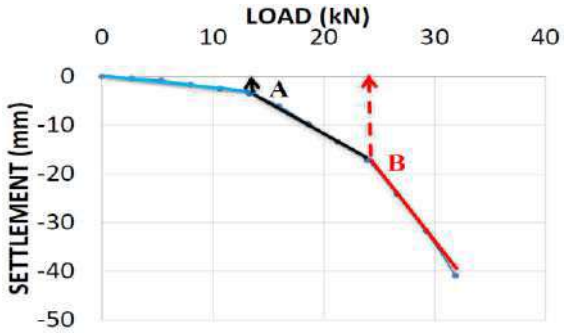


**Fig. 7.** Initial and Final yield load for piled raft foundation as per PDR method

The load-settlement behaviour of a piled raft foundation is considered tri-linear, according to the Poulos-Davis-Randolph (1980) Approach, also known as the PDR method. As illustrated in Fig. 7, the load corresponding to point A is referred to as the "initial yield load" (IYL), at which the piles of PRF yield, whereas the load corresponding to point B is referred to as the "final yield load" (FYL), at which both the raft and the piles of PRF yield [6].

#### 3.1.1 Load settlement behaviour of model unpiled raft foundation

The load settlement curves of a model unpiled raft foundation (UPR) with different shapes of rafts at different relative densities of sand bed are presented in Fig. 8. It was observed that the load carrying capacity of circular rafts was lower than all other shapes at all relative densities. The load settlement characteristics of square, trapezoidal and rectangle shaped rafts were observed quite close to each other.

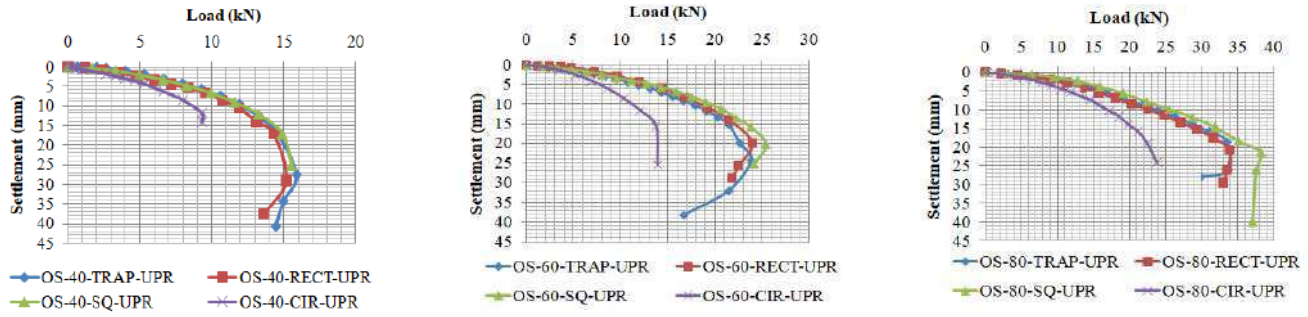


(a) 40% RD (b) 60% RD (c) 80% RD

**Fig. 8.** Load settlement curve of a model unpiled raft (UPR) foundation with different shapes of rafts at different relative densities of sand bed

**Table 4.** Ultimate load of unpiled raft foundation (Qur) with different shape of rafts at different relative density of sand bed (RD)

| RD | Ultimate Load(Qur in kN) | | | | Percentage increment in Qur with respect to Qur of circular raft | | | |
|---|---|---|---|---|---|---|---|---|
| | Square Raft | Circular Raft | Rectangular Raft | Trapezoidal Raft | Square Raft | Circular Raft | Rectangular Raft | Trapezoidal Raft |
| 40% | 14.91 | 9.28 | 13.12 | 12.59 | 61 | 0.00 | 41 | 36 |
| 60% | 25.45 | 10.34 | 23.92 | 23.86 | 146 | 0.00 | 131 | 131 |
| 80% | 38.27 | 17.23 | 33.88 | 33.48 | 122 | 0.00 | 97 | 94 |

From Table 4, it is observed that the minimum and maximum ultimate loads of unpiled raft foundation at all relative densities of sand bed are obtained with a circular and a square raft, respectively. The range of percentage increment in Qur of square, rectangular, and trapezoidal rafts with respect to Qur of circular rafts was found to be 36% to 146%, as shown in Table 4.

### 3.1.2 Load settlement behaviour of model piled raft foundation

Fig. 9 displays the load settlement curve of a model piled raft foundation with different shapes of rafts at different relative densities of sand bed. The load settlement curve of a model piled raft foundation with trapezoidal, rectangular, and square shapes of raft was found to be similar up to a certain limit of load, but at higher loads it can be distinguished. As per the PDR method, the tri-linear behavior of the load settlement curve of a model piled raft foundation was observed, and the load corresponding to the end of the first linear portion where the capacity of piles is assumed to be mobilized is denoted as IYL (Initial Yield Load), and the load corresponding to the end of the second linear portion where the capacity of raft and piles is assumed to be mobilized is termed FYL (Final Yield Load).

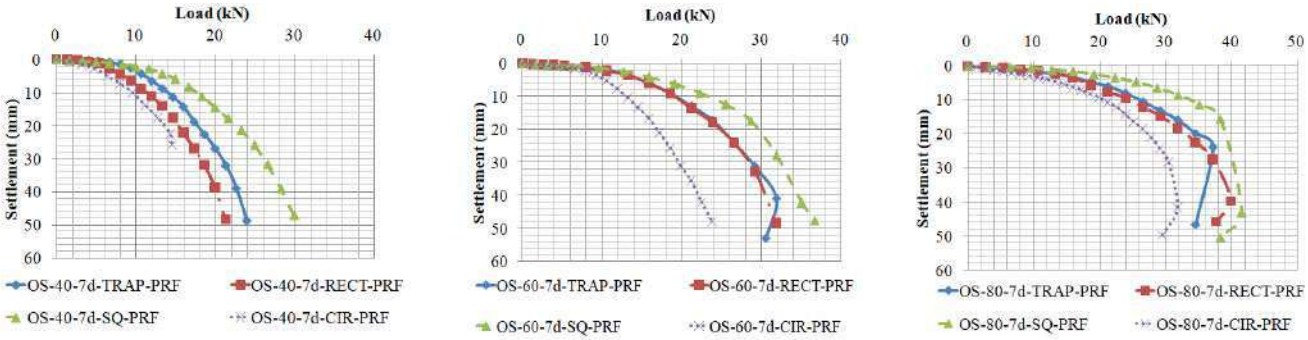


(a) 40% RD (b) 60% RD (c) 80% RD

**Fig. 9.** Load settlement curve of model piled raft foundation with different shape of rafts at different relative densities of sand bed.

### 3.1.2.1 Initial Yield Load (IYL) and Final Yield Load (FYL)

Fig.10 demonstrates the IYL (initial yield load) and FYL (final yield load) of a model piled raft foundation with different shapes of raft and different relative densities of sand bed. It can be observed from Fig. 10 that as the relative density of the sand bed increases, the IYL and FYL increase. In a model piled raft foundation, the IYL and FYL was found to be maximum with a square raft shape and minimum with a circular raft shape at all relative density of sand. The variation in IYL and FYL of MPRF with different shapes of rafts is shown in Table 5.

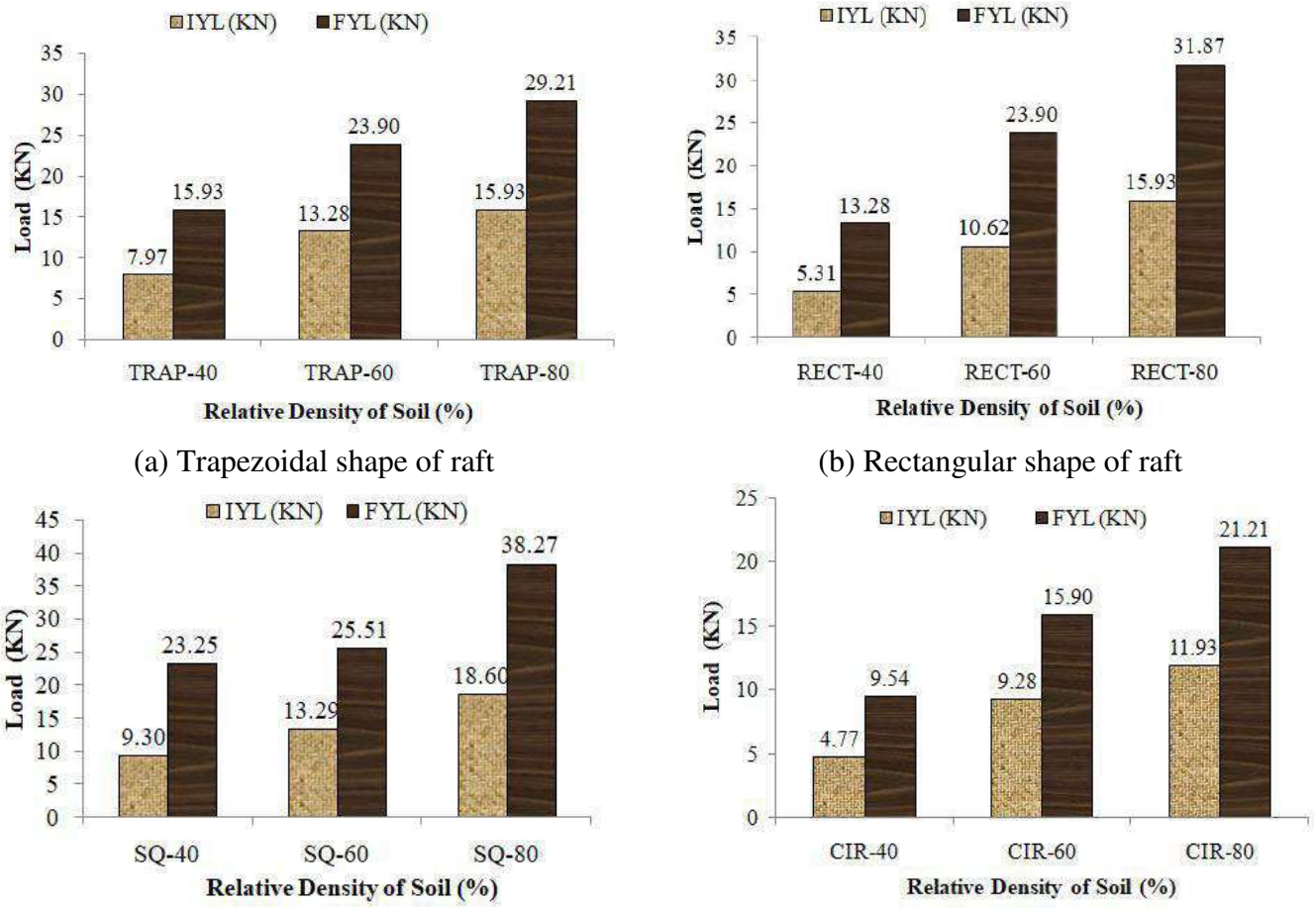


(a) Trapezoidal shape of raft (b) Rectangular shape of raft

(c) Square shape of raft (d) Circular shape of raft

**Fig. 10.** IYL (Initial Yield Load) and FYL (Final Yield Load) of model piled raft foundation with different shape of raft at different relative density of sand bed

**Table 5.** Percentage increment in IYL and FYL of MPRF with different shape of raft as compared to MPRF with Circular shape of raft

| RD of sand bed | Percentage increment in IYL of MPRF with different shapes of raft as compared to MPRF with a circular shape of raft | | | Percentage increment in FYL of MPRF with different shapes of raft as compared to MPRF with a circular shape of raft | | |
|---|---|---|---|---|---|---|
| | TRAP | RECT | SQ | TRAP | RECT | SQ |
| 40% | 67 | 11 | 95 | 67 | 39 | 144 |
| 60% | 43 | 15 | 43 | 50 | 50 | 92 |
| 80% | 34 | 34 | 56 | 38 | 50 | 140 |

### 3.1.3 Load sharing mechanism

The load shared by the two components (pile group and raft) of the MPRF was calculated using EPC readings. The product of EPC readings in kPa and the contact area of respective region in the raft in $m^2$ give the load shared by the raft component in the MPRF, and the difference between the total applied load on the MPRF and the load shared by the raft gives the load shared by the pile group in the MPRF. The load shared by pile group was found to be greater in the initial stage of loading (up to IYL), and after that, increase in the contribution of pile group was found to be less. The proportions of load carried by rafts and pile group are clearly expected to vary as a function of settlement up to IYL and after IYL only the proportion of load carried by raft increased significantly with little improvement in load carrying by pile group[1][8].

Figs. 11 to 14 show load sharing between the pile group and raft in a model piled-raft foundation with different shapes of raft at different relative densities. The load shared by pile group and raft in MPRF with a trapezoidal shape at 40% RD is represented by the OS-40-7d-TRAP-PF and OS-40-7d-TRAP-RF lines, respectively. It is observed that the load shared by pile group is greater at the initial stage of loading up to a relative settlement (s/B) of 0.01 to 0.02 and that after, its contribution becomes less to nil and the contribution of raft increases except in square PRF at 40% RD and circular PRF at 60% RD.

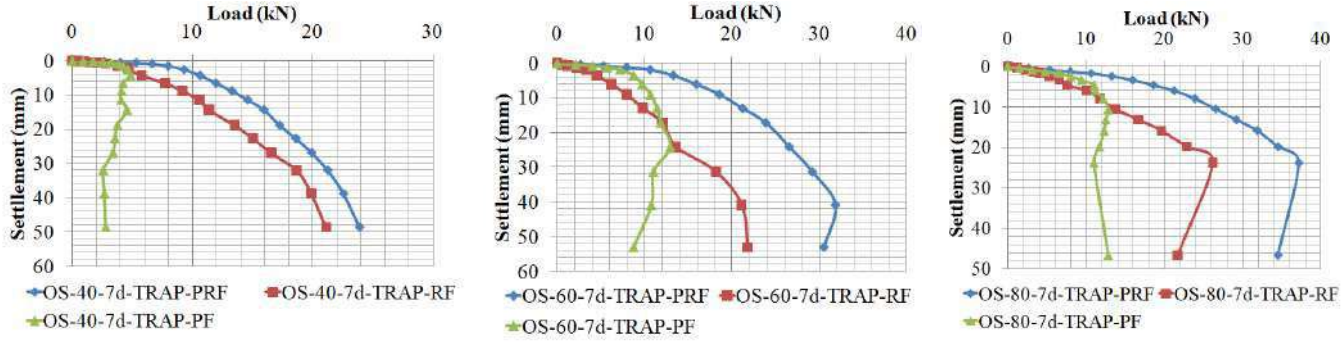


(a) 40% RD (b) 60% RD (c) 80% RD

**Fig. 11.** Load sharing between piles and raft in trapezoidal shaped model piled raft foundation

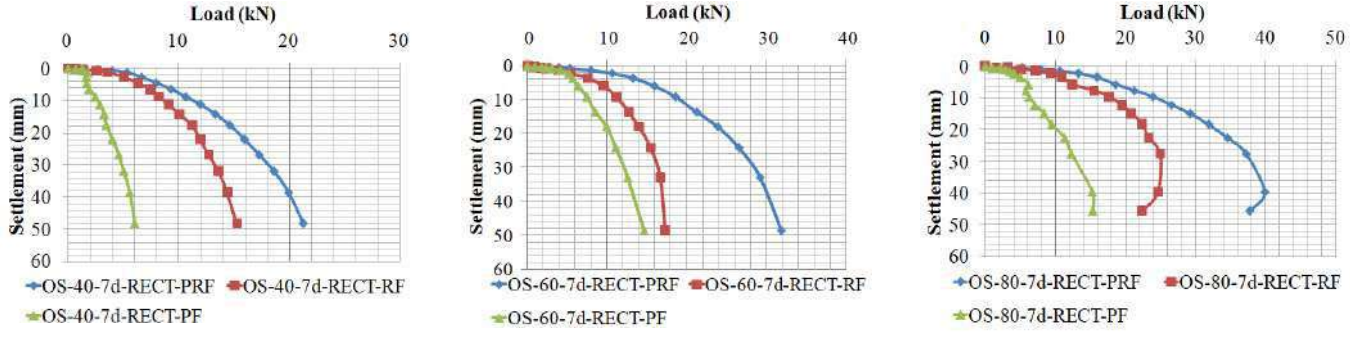


(a) 40% RD (b) 60% RD (c) 80% RD

**Fig. 12.** Load sharing between piles and raft in rectangular shaped model piled raft foundation

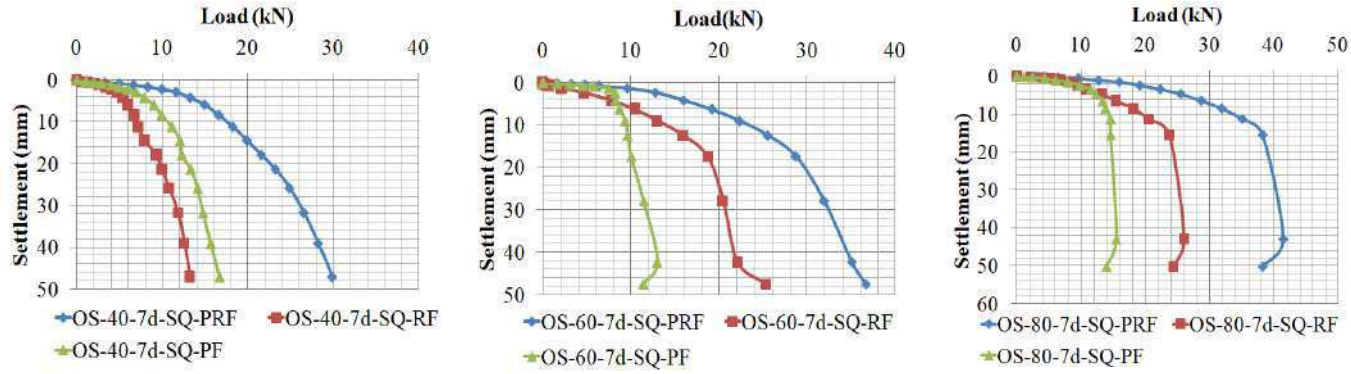


(a) 40% RD (b) 60% RD (c) 80% RD

**Fig. 13.** Load sharing between piles and raft in square shaped model piled raft foundation

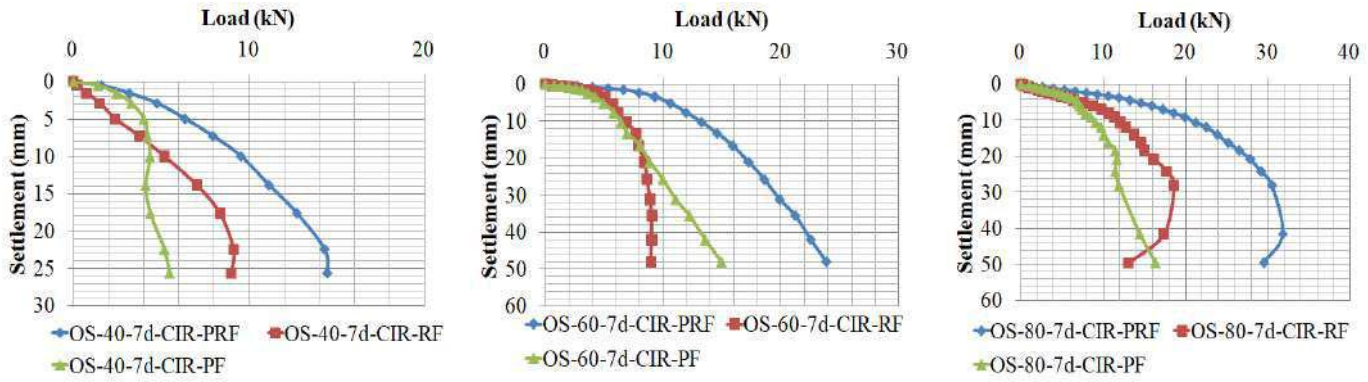


(a) 40% RD (b) 60% RD (c) 80% RD

**Fig. 14.** Load sharing between piles and raft in circular shaped model piled raft foundation

### 3.1.4 Piled raft coefficient:

The ratio of load shared by pile group to the total applied load on a piled raft foundation is known as the piled raft coefficient ($\alpha_p$). It was observed that as the settlement of MPRF increased, the piled raft coefficient decreased, supporting the results obtained by Horikoshi and Randolph [1]. The values of the piled raft coefficient ($\alpha_p$) are higher initially and decrease non-linearly with increasing settlement. Within the initial settlement range, significant decrease in ($\alpha_p$) is observed; up to s/B 0.01 to 0.02 support the results obtained by Junhwan Lee and others [2]. The load shared by pile groups and raft in MPRF, the piled raft coefficient, the relative settlement s/B (ratio of settlement to width of foundation), and variation in the piled raft coefficient at IYL and FYL are presented in Tables 5 and 6, respectively. The maximum value of $\alpha_p$ was found with a circular raft and minimum with a rectangular raft at IYL and 40% RD. At IYL, the $\alpha_p$ of circular and square raft decreases as the relative density of sand increases from 40% to 60%, and it increases from 60% to 80% RD. The $\alpha_p$ of rectangular and trapezoidal raft at IYL increases as the relative density of sand increases from 40% to 60% and decreases for the change in RD from 60% to 80%. The relative settlement (s/B) range for IYL was found to be 0.01 to 0.02.

**Table 5.** Load shared by pile group and raft, $\alpha_p$ and relative settlement (s/B) at IYL

| Shape of raft and relative density | IYL (KN) | Load shared by raft in PRF at IYL | Load shared by piles in PRF at IYL | Piled raft coefficient | Settlement(mm)at IYL | s/B | % Variation in piled raft coefficient w.r.t 40%RD | % Variation in piled raft coefficient w.r.t circular shape of raft |
|---|---|---|---|---|---|---|---|---|
| CIR-40 | 4.77 | 1.24 | 3.53 | 0.74 | 2.92 | 0.01 | 0 | 0 |
| CIR-60 | 9.28 | 5.08 | 4.20 | 0.45 | 3.44 | 0.01 | -39 | 0 |
| CIR-80 | 11.93 | 5.80 | 6.13 | 0.51 | 3.83 | 0.02 | -30 | 0 |
| SQ-40 | 9.30 | 4.34 | 6.29 | 0.59 | 4.12 | 0.019 | 0 | -20 |
| SQ-60 | 13.29 | 6.39 | 6.90 | 0.52 | 2.15 | 0.010 | -12 | +15 |
| SQ-80 | 18.60 | 9.05 | 9.55 | 0.51 | 3.46 | 0.016 | -13 | 0 |
| RECT-40 | 5.31 | 3.53 | 1.78 | 0.33 | 1.20 | 0.01 | 0 | -55 |
| RECT-60 | 10.62 | 5.42 | 5.20 | 0.49 | 2.15 | 0.01 | +46 | +8 |
| RECT-80 | 15.93 | 10.92 | 5.02 | 0.31 | 3.40 | 0.01 | -6 | -39 |
| TRAP-40 | 7.97 | 3.72 | 4.24 | 0.53 | 1.53 | 0.01 | 0 | -28 |
| TRAP-60 | 13.28 | 4.54 | 8.74 | 0.66 | 3.49 | 0.02 | +24 | +46 |
| TRAP-80 | 15.93 | 6.55 | 9.39 | 0.59 | 3.37 | 0.02 | +11 | +15 |

(+) indicates increments and (-) indicates decrements

**Table 6.** Load shared by pile group and raft, $\alpha_p$ and relative settlement (s/B) at FYL

| Shape of raft and relative density | FYL (KN) | Load shared by raft in PRF at FYL | Load shared by piles in PRF at FYL | Piled raft coefficient | Settlement (mm )at FYL | s/B | % Variation in piled raft coefficient w.r.t 40%RD | % Variation in piled raft coefficient w.r.t circular shape of raft |
|---|---|---|---|---|---|---|---|---|
| CIR-40 | 9.54 | 4.33 | 5.21 | 0.55 | 10.02 | 0.04 | 0 | 0 |
| CIR-60 | 15.90 | 7.88 | 8.03 | 0.50 | 16.70 | 0.07 | -8 | 0 |
| CIR-80 | 21.21 | 12.13 | 9.08 | 0.43 | 10.71 | 0.04 | -22 | 0 |
| SQ-40 | 23.25 | 7.96 | 10.65 | 0.57 | 12.31 | 0.06 | 0 | 5 |
| SQ-60 | 25.51 | 13.26 | 8.00 | 0.38 | 17.91 | 0.08 | -34 | -25 |
| SQ-80 | 38.27 | 19.74 | 12.15 | 0.38 | 15.50 | 0.07 | -33 | -11 |
| RECT-40 | 13.28 | 10.03 | 3.25 | 0.25 | 14.13 | 0.08 | 0 | -55 |
| RECT-60 | 23.90 | 13.96 | 9.94 | 0.42 | 17.91 | 0.10 | +70 | -18 |
| RECT-80 | 31.87 | 22.42 | 9.45 | 0.30 | 18.19 | 0.10 | +21 | -31 |
| TRAP-40 | 15.93 | 11.37 | 4.56 | 0.29 | 14.33 | 0.08 | 0 | -48 |
| TRAP-60 | 23.90 | 12.03 | 11.87 | 0.50 | 17.14 | 0.10 | +73 | -2 |
| TRAP-80 | 29.21 | 16.71 | 12.50 | 0.43 | 13.16 | 0.07 | +49 | 0 |

(+) indicates increments and (-) indicates decrements

### 3.1.5 Comparison of behaviour of Unpiled raft and piled raft foundation:

The load settlement behaviour of a model unpiled raft foundation and a piled raft foundation was compared by comparing the load taken by the model unpiled raft foundation and the piled raft foundation at the same settlement value. The increment in load taken by the model piled raft foundation compared to the unpiled raft foundation was calculated in percentage and is denoted by PIL in Tables 7, 8, and 9. From the results, it can be observed that at very low relative settlement and at very high relative settlement the difference between the load carrying capacity of MPRF and UPR is higher and the difference decreases at intermediate relative settlement and with increase in the relative density.

**Table 7.** Percentage increase in load taken by MPRF as compared to UPR at 40% relative density

| s/B | Settlement (mm) | Shape of raft and relative density | | | | | | | | | | | |
|---|---|---|---|---|---|---|---|---|---|---|---|---|---|
| | | TRAP-40 | | | RECT-40 | | | SQ-40 | | | CIR-40 | | |
| | | Qr (kN) | Qprf (kN) | PIL | Qr (kN) | Qprf (kN) | PIL | Qr (kN) | Qprf (kN) | PIL | Qr (kN) | Qprf (kN) | PIL |
| 0.025 | 5.5 | 9.11 | 11.34 | 24 | 8.41 | 8.68 | 3 | 8.88 | 14.56 | 64 | 6.10 | 6.71 | 10 |
| 0.05 | 11 | 12.53 | 14.40 | 15 | 12.04 | 12.06 | 0 | 12.65 | 18.17 | 44 | 8.97 | 9.95 | 11 |
| 0.075 | 16.5 | 14.44 | 16.57 | 15 | 14.07 | 14.19 | 1 | 14.71 | 20.93 | 42 | 9.28 | 12.25 | 32 |
| 0.1 | 22 | 15.20 | 18.36 | 21 | 14.65 | 15.93 | 9 | 15.31 | 23.51 | 54 | 9.28 | 14.17 | 53 |
| 0.125 | 27.5 | 15.89 | 20.08 | 26 | 15.04 | 17.44 | 16 | 16.98 | 25.38 | 49 | 9.28 | 15.53 | 67 |

Where,
**Qr** = Load on model unpiled raft foundation (UPR),
**Qprf** = Load on MPRF,
**PIL** = percentage increment in load taken by MPRF with respect to UPR

**Table 8.** Percentage increase in load taken by MPRF as compared to UPR at 60% relative density

| s/B | Settlement (mm) | Shape of raft and relative density | | | | | | | | | | | |
|---|---|---|---|---|---|---|---|---|---|---|---|---|---|
| | | TRAP-60 | | | RECT-60 | | | SQ-60 | | | CIR-60 | | |
| | | Qr (kN) | Qprf (kN) | PIL | Qr (kN) | Qprf (kN) | PIL | Qr (kN) | Qprf (kN) | PIL | Qr (kN) | Qprf (kN) | PIL |
| 0.025 | 5.5 | 12.30 | 15.37 | 25 | 13.76 | 18.44 | 34 | 14.03 | 18.07 | 29 | 8.11 | 10.76 | 33 |
| 0.05 | 11 | 18.45 | 19.90 | 8 | 19.27 | 25.45 | 32 | 20.47 | 24.27 | 19 | 11.72 | 13.54 | 16 |
| 0.075 | 16.5 | 21.81 | 23.49 | 8 | 22.55 | 30.55 | 36 | 24.09 | 28.14 | 17 | 13.80 | 15.83 | 15 |
| 0.1 | 22 | 23.24 | 25.76 | 11 | 23.38 | 34.26 | 47 | 24.41 | 30.11 | 23 | 13.90 | 17.49 | 26 |
| 0.125 | 27.5 | 22.86 | 27.81 | 22 | 22.06 | 37.19 | 69 | 24.18 | 31.79 | 31 | 15.13 | 18.97 | 25 |

**Table 9.** Percentage increase in load taken by MPRF as compared to UPR at 80% relative density

| s/B | Settlement (mm) | Shape of raft and relative density | | | | | | | | | | | |
|---|---|---|---|---|---|---|---|---|---|---|---|---|---|
| | | TRAP-80 | | | RECT-80 | | | SQ-80 | | | CIR-80 | | |
| | | Qr (kN) | Qprf (kN) | PIL | Qr (kN) | Qprf (kN) | PIL | Qr (kN) | Qprf (kN) | PIL | Qr (kN) | Qprf (kN) | PIL |
| 0.025 | 5.5 | 16.82 | 20.33 | 21 | 15.97 | 18.44 | 15 | 18.94 | 26.93 | 42 | 12.18 | 14.94 | 23 |
| 0.05 | 11 | 25.14 | 27.05 | 8 | 24.08 | 25.45 | 6 | 27.14 | 34.73 | 28 | 17.80 | 21.51 | 21 |
| 0.075 | 16.5 | 31.59 | 32.32 | 2 | 30.60 | 30.55 | 0 | 33.50 | 38.38 | 15 | 21.46 | 25.30 | 18 |
| 0.1 | 22 | 33.59 | 35.98 | 7 | 33.81 | 34.26 | 1 | 38.17 | 39.02 | 2 | 23.33 | 28.28 | 21 |
| 0.125 | 27.5 | 30.49 | 36.75 | 21 | 33.70 | 37.19 | 10 | 37.56 | 39.66 | 6 | 23.86 | 30.26 | 27 |

## 4. Conclusion

From this research work, the following conclusions were drawn:

1. The square shape of the raft is most preferable amongst the rafts studied in this study for unpiled rafts as well as piled raft foundations because its load-carrying capacity, or IYL and FYL, is found to be highest at all relative densities.
2. The circular shape of the raft is least preferable amongst the rafts studied in this study for unpiled rafts as well as piled raft foundations because its load-carrying capacity, or IYL and FYL, is found to be lowest at all relative densities.
3. The piled raft coefficient at IYL is found to be maximum in circular MPRF at 40% RD, and at 60% and 80% RD, it is found to be maximum in trapezoidal MPRF. i.e., at 40% RD, the contribution of piles in sharing the load applied on circular MPRF is greater, and at 60% and 80% RD, it is found to be greater in trapezoidal MPRF at IYL. The piled raft coefficient at FYL is found at its maximum in circular MPRF at all relative densities. i.e., the contribution of pile groups is found to be higher in circular MPRF as compared to other shapes of MPRF at FYL.
4. The PIL is found to be negligible in rectangular MPRF at 40% and 80% RD. i.e., at 40% and 80% RD, a rectangular raft is preferable to a rectangular PRF.

## 5. Acknowledgement

Partial financial support for this research work was received from the DST PURSE (Department of Science and Technology—Promotion of University Research and Scientific Excellence (Phase 2)) grant under grant agreement no. SR/PURSE Phase-2/28(G) dated 10/08/2018. The earth pressure cells and their indicator used in this research were purchased under this grant.

## Abbreviations and Acronyms

| | | |
|---|---|---|
| *s/B* | : | ratio of settlement to width of model raft (relative settlement) |
| *7d* | : | Center-to-center distance between piles of a pile group in MPRF = 7 d (d = external diameter of pile) |
| Qp,u | : | Ultimate pile load capacity |
| Qprf | : | Load on MPRF |
| Qr | : | Load on model unpiled raft foundation (URF) |
| Qur | : | Ultimate load of unpiled raft foundation |
| $\alpha_p$ | : | Piled raft coefficient |
| $\phi$ | : | Angle of internal friction of sand bed (degree) |
| $\gamma_d$ | : | Dry unit weight (kN/m$^3$) |
| *CIR* | : | *Circular shape of raft* |
| *EPC* | : | *Earth pressure cell* |
| *FYL* | : | *Final Yield Load (kN)* |
| *IYL* | : | *Initial Yield Load (kN)* |
| *MPRF* | : | *Model Piled raft foundation* |
| *OS-40, OS-60, OS-80* | : | *Orsang sand with 40%, 60 %, 80 % RD* |
| *PF* | : | *Load shared by pile group in MPRF* |
| *PIL* | : | *percentage increment in load taken by MPRF with respect to UPR* |
| *PRF* | : | *Total load applied on MPRF* |
| *RD* | : | *Relative density* |
| *RECT* | : | *Rectangular shape of raft* |
| *RF* | : | *Load shared by raft in MPRF* |
| *SQ* | : | *Square shape of raft* |
| *TRAP* | : | *Trapezoidal shape of raft* |
| *UPR* | : | *Unpiled raft foundation* |
| *UR* | : | *Unpiled raft* |

## References

[1] Horikoshi K, Randolph MF. Centrifuge modelling of piled raft foundations on clay. Geotechnique 1996; 46(4):741–52.

[2] Lee J, Park G, Park K. Estimation of load-sharing ratios for piled rafts in sands that includes interaction effects. Comput Geotech. 2015; 63:306–314.

[3] Jaymin D Patil, Sandeep A Vasanwala, Chandresh H Solanki. An experimental investigation on behavior of piled raft foundation. International Journal of Geomatics and Geosciences.2014; 5(2):300-311

[4] Cooke R.W. Piled raft foundations on stiff clays,Contribution to design Philosophy. Geotechnique, 1986;35(2):169-203

[5] Lee S.H.,and Chung C.K. An experimental study of the interaction of vertical loaded pile groups in sand.Canadian Geotechnical Journal. 2005; 42:1485-1493.

[6] Poulos H.G.Piled raft foundations: Design and applications. Geotechnique. 2001; 51(2): 95–113.

[7] El Sawwaf, Mostafa. Experimental study of eccentrically loaded raft with connected and unconnected short piles. Journal of Geotechnical and Geoenvironmental engineering, 2010;136(10): 1394-1402.

[8] Lee, Junhwan, Donggyu Park, and Kyujin Choi. Analysis of load sharing behavior for piled rafts using normalized load response model. Computers and Geotechnics,2014; 57:65-74

# 3 Assessment of Effect of Vehicular Emissions on Kanpur City Using Vulnerability Analysis

**Varun Yadav*, Rajiv Ganguly**

Department of Civil Engineering, Harcourt Butler Technical University, Kanpur, Uttar Pradesh, India.

*Corresponding Author Email: rganguly@hbtu.ac.in

## Abstract

Emerging economies have improved due to rapid urbanization and industrialization, often causing environmental issues. Air Pollution is one of the major environmental problems experienced due to this phenomenon. The problem is further compounded due to increase in number of vehicles leading to increase in air pollutants concentrations. This study examines the effects of vehicular emissions on urban air quality and public health focusing on the impacts of the air pollution. In particular, a vulnerable analysis (VA) has been presented for Kanpur city. The VA was conducted for the study period of five months for the year 2021 wherein the data was collected from eight sites in Kanpur City. The pollutants considered for the study was $PM_{10}$, $SO_2$ and $NO_2$. It was observed from the study that the average concentrations of $PM_{10}$ exceeded the NAAQS standards at all of the sites. However, the average concentrations $SO_2$ were found to be well within the prescribed standards. The average concentrations of $NO_2$ were exceeded at 5 of the 8 selected locations. The pollutant $PM_{10}$ was primarily responsible for raising the vulnerability index of Kanpur city.

**Keywords**

Kanpur; $NO_2$; $PM_{10}$; Vehicular Emissions; Vulnerability Index.

Received: 31 May 2023 | Accepted: 20 Sep 2023 | Online: 28 Sep 2023

**Cite this article**

Varun Yadav and Rajiv Ganguly (2023). Assessment of Effect of Vehicular Emissions on Kanpur City Using Vulnerability Analysis. *Engineering Research Transcripts*, 3, 25–31.

DOI: https://doi.org/10.55084/grinrey/ERT/978-81-964105-0-6_3

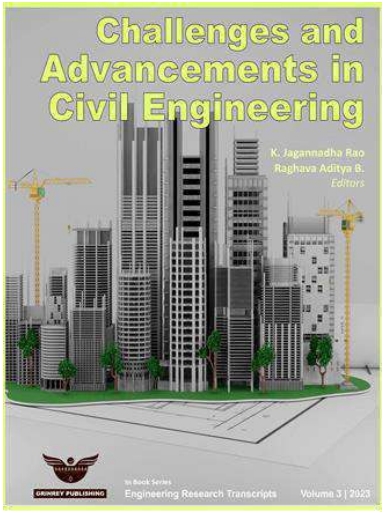

## 1. Introduction

India is one of the most developing countries in the world, outpacing the development of many developed countries. This rapid development of the country has been bought about by increased industrialization and urbanization processes [1]. However, such rapid pace of industrialization and urbanization, places a great strain on the existing natural resources. Due to such increased anthropogenic activities of industrial and vehicular emissions leads to significant deterioration of ambient air quality. With improved regulatory guidelines and interventions, there has been a significant reduction in air pollutants arising from industries; however with increased urbanization, a huge surge has been observed in use of personal motor vehicles [2]. This has led to substantial increase in air pollution due to emissions from vehicular exhausts. These pollutants emitted from vehicular emissions undergoing secondary reactions in the ambient air have significant effects on human health [3-5]. In this context, vehicles plying on the road following stricter emission norms could significantly reduce the pollutant concentrations. However, the increased number of vehicles on the road could offset the potential environmental benefits [6-7]. Hence, the potential effect of pollutants on the ambient air needs to be assessed. There exist different techniques for determination of exposure of air pollutants including implementation of large scale monitoring systems and Air Quality (AQ) modelling techniques for assessments. Both the methods have their own advantages and disadvantages, for example while monitoring data fails to represent spatial variation in data, the accuracy of the Air Quality (AQ) dispersion models are highly dependent on the quality of the input parameters [8]. The Vulnerability Index is another indices used to represent the effect of air pollutants on human health [9-10]. Reported studies conducted at megacity of Delhi showed that the vulnerability indexes (VI) were *low* at residential areas and *medium to high* on intersections and highways [10]. In similar manner, a study conducted in the traffic intersections of major areas in Kolkata scored *high* on the vulnerability index (VI) for all of the selected study intersections [9].

In the above context, the main objectives of the study were (a) to observe the variation in monitored concentrations of air pollutants from selected sites of Kanpur city for five months of 2021 and (b) to evaluate the VI at the selected sites covering the same study periods. The selected method of analysis has not been applied before at the study area and is another possible way of representing air quality scenario in Kanpur city.

## 2. Material and methods

### 2.1 Secondary Air Quality Data Collection

India has a wide network of air quality monitoring stations that are used for recording data. In Kanpur, the National Ambient Monitoring Program (NAMP) currently operates eight manual monitoring stations as shown in Table 1. This study compiles the data from the website of the Uttar Pradesh Pollution Control Board (UPPCB) on the five-month air quality trend for the three primary pollutants $PM_{10}$, $SO_2$, and $NO_2$. The major sources of air pollution in Kanpur city can be attributed to five different categories namely fugitive dust sources, domestic, transport (motor vehicles and railways), commercial, and industrial activities.

### 2.2 Vulnerability Analysis (VA)

Vulnerability analysis is carried out to determine the effects of air pollutants on human health at the selected study locations [9-10]. The information arising out of the VA is to help in planning and implementation of suitable mitigation measures for air pollution. A total vulnerable score (VST) can be obtained from the following expression:

$$\text{VST} = \sum_{i=1}^{n} Xi\, Ti \quad (1)$$

where $Xi$ is the concentration of $i^{th}$ air pollutant, $Ti$ the toxicity weighing factors for $i^{th}$ air pollutant, and $n$ the number of air pollutants. The toxicity weighing factors in this analysis are from World Bank (1992) as given below in Table 2.

**Table 1**: List of monitoring stations in Kanpur city (http://www.uppcb.com/ambient_quality.htm)

| Location | Monitoring station number | Type of station |
|---|---|---|
| Kidwai Nagar | S1 | Residential |
| Jareeb Chowki | S2 | Commercial |
| Panki Site 1 | S3 | Industrial |
| Shashtri Nagar | S4 | Residential |
| Awas Vikas Kalyanpur | S5 | Residential |
| Dada Nagar | S6 | Residential |
| IIT Campus | S7 | Residential |
| Ramadevi | S8 | Commercial |

**Table 2**: Pollutants and their relative weights [9-10]

| Sr. No. | Pollutant | Relative weight |
|---|---|---|
| **1.** | $NO_x$ | 4.5 |
| **2.** | $PM_{10}$ | 2.3 |
| **3.** | $SO_2$ | 1.4 |

The Vulnerability index (VI) has been calculated based on VTr of threshold concentrations for residential and sensitive areas and is summarized in Table 3.

**Table 3**: Rating Scale for Vulnerability Index [9-10]

| Sr. No. | Total vulnerability score (VST) | Vulnerability index (VI) |
|---|---|---|
| **1** | >4420 | Very high |
| **2** | 4420–3315 | Medium high |
| **3** | 3315–2210 | High |
| **4** | 2210–1661 | Medium high |
| **5** | 1661–1113 | Medium |
| **6** | 1113–517 | Low |
| **7** | <517 | Very Low |

## 3. Results

### 3.1 Air Quality Data Analysis

Table 4 summarizes the average concentration of $PM_{10}$ ($\mu g/m^3$) for the first five months of the year 2021. It was observed from Table 4 that sites S2, S6 and S8 experienced the maximum concentrations of $PM_{10}$ due to large flow of diesel vehicles passing through these monitoring regions. Further, high concentrations of the pollutant were observed in the month of January at all of the sites during winter season. This may be

attributed to inversion effects during winter season. The average concentration of the pollutants varying at the different monitoring sites over the five-month study period has been summarized in Fig. 1.

**Table 4**: Average concentrations of $PM_{10}$ ($\mu g/m^3$) for the study period

| STATION/MONTHS | JANUARY | FEBRUARY | MARCH | APRIL | MAY | AVERAGE |
|---|---|---|---|---|---|---|
| S1 | 250.53 | 223.46 | 163.18 | 151.2 | 115.41 | 180.75 |
| S2 | 328.61 | 198.45 | 184.05 | 177.65 | 122.44 | **202.24** |
| S3 | 308.24 | 169.37 | 202.87 | 177.42 | 136.83 | 198.94 |
| S4 | 299.93 | 147.96 | 134.28 | 135.96 | 100.62 | 163.75 |
| S5 | 290.28 | 176.21 | 146.7 | 122.63 | 94.32 | 166.02 |
| S6 | 380 | 429.8 | 569.2 | 305 | 0 | **336.8** |
| S7 | 175 | 182.1 | 126.1 | 175.8 | 0 | 131.8 |
| S8 | 329.8 | 328 | 316 | 339.6 | 0 | **262.68** |

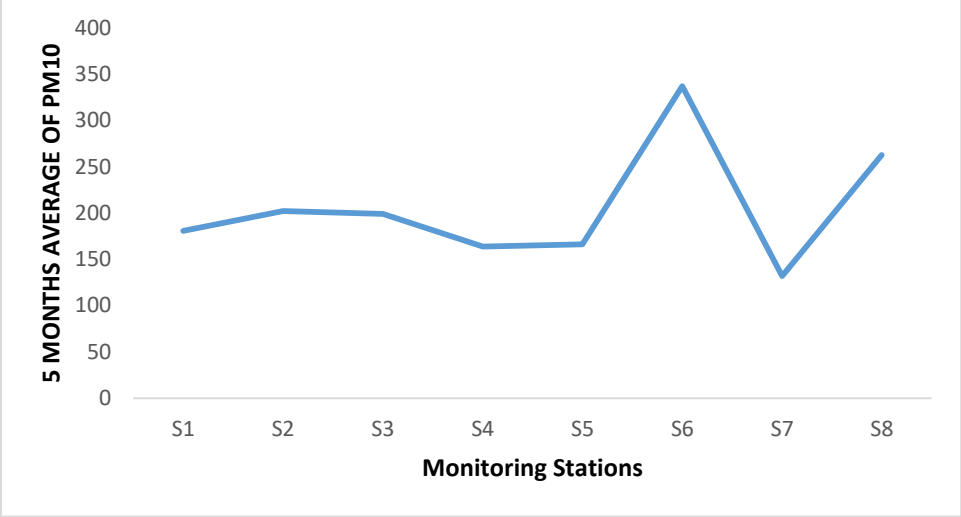


**Fig. 1.** Average concentrations of $PM_{10}$ at the monitoring locations.

Table 5 presents the average concentrations of $SO_2$ for the study period in the year 2021. It was observed from Table 5 that the average concentrations $SO_2$ at all the monitoring stations were less than the prescribed NAAQS standards. This suggests that the $SO_2$ concentrations recorded at the monitoring sites may be attributed to existing background concentrations without the influence of any sufficient anthropogenic activities. The average concentration of the pollutant varying at the different monitoring sites over the five-month study period has been summarized in Fig. 2.

**Table 5**: Average concentrations of $SO_2$ ($\mu g/m^3$) for the study period

| STATION/MONTHS | JANUARY | FEBRUARY | MARCH | APRIL | MAY | AVERAGE |
|---|---|---|---|---|---|---|
| S1 | 16.89 | 20.34 | 8.66 | 8.5 | 7.76 | 12.43 |
| S2 | 14.62 | 15.58 | 9.84 | 9.08 | 7.68 | 11.36 |
| S3 | 18.44 | 17.73 | 9.89 | 10.59 | 9.27 | **13.184** |
| S4 | 16.61 | 12.71 | 11.49 | 9.28 | 7.53 | 11.524 |
| S5 | 13.92 | 14.41 | 9.8 | 12.96 | 7.43 | 11.704 |
| S6 | 5.4 | 2 | 2 | 4.4 | 0 | 2.76 |
| S7 | 2 | 2 | 2 | 2 | 0 | 1.6 |
| S8 | 2 | 4.2 | 4.1 | 2 | 0 | 2.46 |

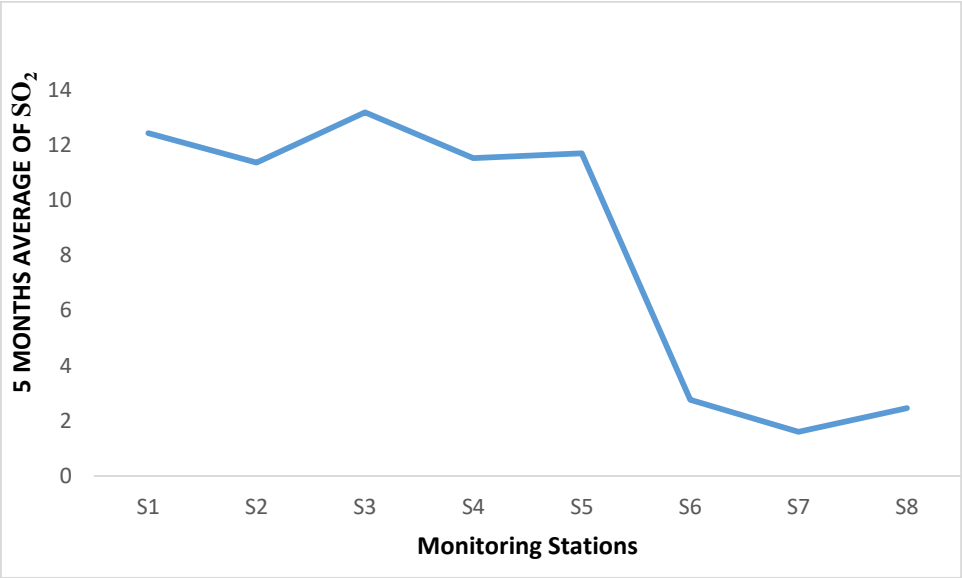


**Fig. 2.** Average concentrations of $SO_2$ at the monitoring locations

Table 6 presents the average concentrations of $NO_2$ for the study period in the year 2021. This study shows the number of locations exceeding the NAAQS standards (40 µg/m3) with respect to $NO_2$ which may be due to the Industrial and Commercial activities. The average concentration of the pollutant varying at the different monitoring sites over the five-month study period has been summarized in Fig. 3.

**Table 6**: Average concentrations of $NO_2$ (µg/$m^3$) for the study period

| STATION/MONTHS | JANUARY | FEBRUARY | MARCH | APRIL | MAY | AVERAGE |
|---|---|---|---|---|---|---|
| S1 | 68.77 | 87.35 | 51.85 | 48.95 | 39.5 | **59.284** |
| S2 | 71 | 78.91 | 55.04 | 55.16 | 40.65 | **60.152** |
| S3 | 85.5 | 86.94 | 58.01 | 64.37 | 40.65 | **67.094** |
| S4 | 76.13 | 72.52 | 50.21 | 35.53 | 35.99 | **54.076** |
| S5 | 66.25 | 76.31 | 53.85 | 53 | 34.06 | **56.694** |
| S6 | 39.3 | 30.5 | 32.1 | 43.2 | 0 | 29.02 |
| S7 | 9.5 | 9.4 | 10.8 | 8.6 | 0 | 7.66 |
| S8 | 30.6 | 39.9 | 39.9 | 35.5 | 0 | 29.18 |

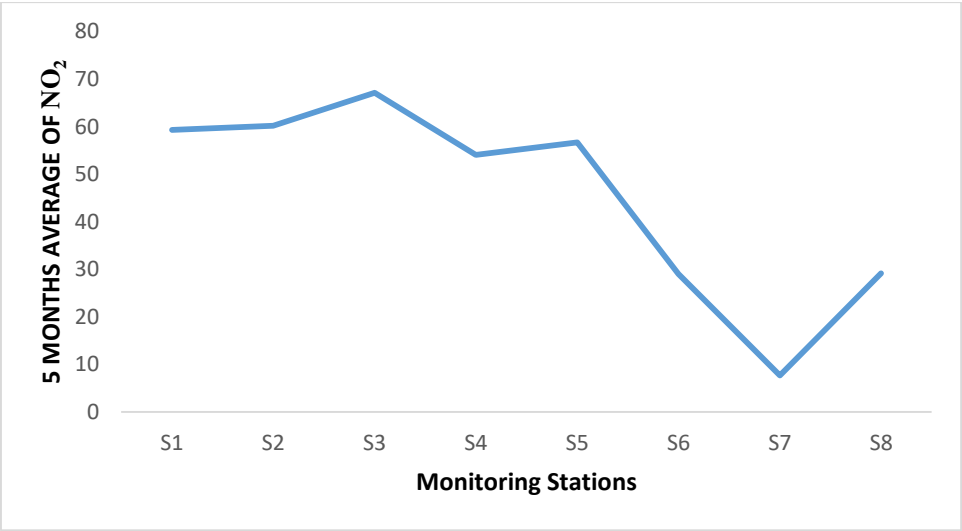


**Fig. 3.** Average concentrations of $NO_2$ at the monitoring locations

### 3.2 Vulnerability Analysis (VA)

From the Table 8, it can be analyzed that the Vulnerability index (VI) is rated low at almost all locations. The maximum VI is observed at Station 6 and minimum at Station 7. The VI was carried out on the basis of 3 monitored parameters in Kanpur city. However, studies conducted in Kolkata [9] and Delhi [10] was based on a total of 6 monitored parameters. The present study did not include the parameters like CO, Pb, etc. for Kanpur sites due to unavailability of monitoring data. To further study this effect, a revised table (Table 7) is presented for Delhi location wherein the VI was recalculated on the basis of the same parameters as observed for Kanpur city. It was observed from the revised VI that there was a change in grading by one scale at a minimum at the sites in Delhi. In some locations, the change in scale was observed to by two scales also. This implies that based on the results presented in Table 7, the results obtained for Kanpur city needs to be upscaled by at least one scale to represent the actual ambient air quality. This is presented in Table 8 as revised VI scale.

**Table 7:** Example Set of Data from the Case of Delhi

| | | **CO** | **$NO_2$** | **SO 2** | **RSP M** | **SPM** | **Pb** | **$VS_T$** | **VI (Jain and Khare, 2008)** | **Revised $VS_T$ [$VS_T$-(CO+Pb +RSPM)]** | **Revised VI** |
|---|---|---|---|---|---|---|---|---|---|---|---|
| 2003 | ITO | 124 | 743.2 | 14.6 | 632.5 | 330.4 | 3.14 | **1848** | Mh | **1088.36** | Low |
| | Sirifort | 88 | 281.4 | 5.8 | 391 | 276.5 | 1.95 | **1045** | Low | **564.05** | Low |
| | Nizamuddin | 95.5 | 194.9 | 17.1 | 299 | 283.5 | 1.61 | **892** | Low | **495.89** | Very low |
| | Ashok Vihar | 55.3 | 144.9 | 8.5 | 303.6 | 320.4 | 2.21 | **835** | Low | **473.89** | Very low |
| | Janakpuri | 68.4 | 198.9 | 16.4 | 315.1 | 261.9 | 1.36 | **862** | Low | **477.14** | Very low |
| | Netaji Nagar | 90.4 | 208.8 | 10.1 | 349.6 | 316.8 | 2.46 | **978** | Low | **535.54** | Low |
| | Townhall | 98.6 | 265.1 | 16.1 | 522.1 | 430.2 | 3.57 | **1336** | Medium | **711.73** | Low |
| 2004 | Ito | 103.4 | 836.1 | 15.5 | 572.7 | 289.3 | 4.16 | **1821** | Mh | **1140.74** | Medium |
| | Sirifort | 57.6 | 358.7 | 7.1 | 349.6 | 258.4 | 2.55 | **1034** | Low | **624.25** | Low |
| | Nizamuddin | 80.5 | 194.9 | 17.1 | 269.1 | 283.5 | 2.72 | **848** | Low | **495.68** | Very low |
| | Ashok Vihar | 49.6 | 144.9 | 8.5 | 223.1 | 320.4 | 2.89 | **749** | Low | **473.41** | Very low |
| | Janakpuri | 53.7 | 198.9 | 16.4 | 257.6 | 261.9 | 1.19 | **790** | Low | **477.51** | Very low |
| | Netaji Nagar | 78.2 | 208.8 | 10.1 | 292.1 | 316.8 | 3.31 | **909** | Low | **535.39** | Low |
| | Townhall | 85.4 | 265.1 | 16.1 | 455.4 | 430.2 | 3.65 | **1256** | Medium | **711.55** | Low |

**Source:** https://doi.org/10.1007/s10661-007-9681-7 [10]

**Table 8**: Total Vulnerability Score ($VS_T$)

| **STATIONS** | **Vulnerability Scores (VS)** | | | **$VS_T$** | **VI** | **Revised VI** |
|---|---|---|---|---|---|---|
| | $PM_{10}$ | $SO_2$ | $NO_2$ | | | |
| S1 | 180.756 | 12.43 | 59.284 | 699.92 | Low | Medium |
| S2 | 202.24 | 11.36 | 60.152 | 751.74 | Low | Medium |
| S3 | 198.946 | 13.184 | 67.094 | 777.96 | Low | Medium |
| S4 | 163.75 | 11.524 | 54.076 | 636.10 | Low | Medium |
| S5 | 166.028 | 11.704 | 56.694 | 653.37 | Low | Medium |
| S6 | 336.8 | 2.76 | 29.02 | 909.09 | Low | Medium |
| S7 | 131.8 | 1.6 | 7.66 | 339.85 | Very Low | Low |
| S8 | 262.68 | 2.46 | 29.18 | 738.92 | Low | Medium |

## 4. Conclusion

This study reveals that air pollution is a significant problem in Kanpur city. The increased levels of air pollution at different monitoring stations in the city, which are primarily caused by vehicular sources, are a serious reason for concern. Further, high concentration of Particulate matter show plying of large number of diesel vehicles within the city premises make it unhealthy for the residents. This suggests that a comprehensive emission inventory for these pollutants needs to be prepared for developing successful air quality management strategy for the city. It is important to maintain a detailed record of all vehicles (particularly diesel vehicles) so that they can be phased out at the end of their life span thereby reducing pollutant emissions.

### References

[1] EEA (European Environmental Agency). 2013. "Air quality in Europe 2013 report." Accessed June 25, 2019. https://www.eea.europa.eu.

[2] Ganguly, R., Sharma, D., Kumar, P., & Gurjar, B. R. (2021). Dispersion modeling of air pollutants in a hilly city in India. *Journal of Hazardous, Toxic, and Radioactive Waste*, *25*(2), 04020073. https://doi.org/10.1061/(ASCE)HZ.2153-5515.0000574

[3] Montone, R. A., Camilli, M., Russo, M., Termite, C., La Vecchia, G., Iannaccone, G., ... & Niccoli, G. (2022). Air pollution and coronary plaque vulnerability and instability: an optical coherence tomography study. *Cardiovascular Imaging*, *15*(2), 325-342. https://doi.org/10.1016/j.jcmg.2021.09.008.

[4] Ganguly, R., and B. M. Broderick. 2008. "Performance evaluation and sensitivity analysis of the general finite line source model for CO concentrations for motorways in Ireland: A note." Transp. Res. 13 (3): 198–205. https://doi.org/10.1016/j.trd.2008.01.006

[5] Guttikunda, S. K., and R. Goel. 2013. "Health impacts of particulate pollution in a megacity-Delhi, India." Environ. Dev. 6: 8–20. https://doi.org/10.1016/j.envdev.2012.12.002

[6] Brusselaers, N., Macharis, C., & Mommens, K. (2023). The health impact of freight transport-related air pollution on vulnerable population groups. *Environmental Pollution*, *329*, 121555. https://doi.org/10.1016/j.envpol.2023.121555.

[7] Hama, S. M. L., P. Kumar, R. M. Harrison, W. J. Bloss, M. Khare, S.Mishra, A. Namdeo, R. Sokhi, P. Goodman, and C. Sharma. 2020."Four-year assessment of ambient particulate matter and trace gasesin the Delhi-NCR region of India." Sustainable Cities Soc. 54:102003. https://doi.org/10.1016/j.scs.2019.102003.

[8] Ganguly, R., S. Batterman, V. Isakov, M. Snyder, M. Breen, J. Burke,and W. Brakefield-Caldwell. 2015. "Effects of geocoding errors on traffic related air pollutant exposure and concentration estimates." J. Exposure Sci. Environ. Epidemiol. 25 (5): 490–498. https://doi.org/10.1038/jes.2015 .1

[9] Ghose Mrinal, K., R. Paul, and S. K. Banerjee. "Assessment of the impacts of vehicular emissions on urban air quality and its management in Indian context: the case of Kolkata." *Environ Sci Policy* 7.4 (2004): 345-351. https://doi.org/10.1016/j.envsci.2004.05.004

[10] Jain, Suresh, and Mukesh Khare. "Urban air quality in mega cities: a case study of Delhi City using vulnerability analysis." Environmental monitoring and assessment 136.1 (2008): 257-265. https://doi.org/10.1007/s10661-007-9681-7

# 4 Compliance of Vehicular Emission Norms in Kanpur City, India

**Harshit Verma, Dipteek Parmar, Rajiv Ganguly***

Department of Civil Engineering, Harcourt Butler Technical University, Nawabganj, Kanpur, India

Email: hv8960@gmail.com, d_parmar@rediffmail.com, *rganguly@hbtu.ac.in

## Abstract

Due to the rising urbanisation, there are significantly more motor vehicles on the road, which has caused a huge increase in vehicle emissions. This study intends to determine the percentage of monitored automobiles in Kanpur, India, that abide by Bharat Stage-IV and VI (BS-IV and VI) emission criteria. For a four-month period in 2018, the transport department's pollution under control (PUC) certificate at a gasoline station was utilized for collecting secondary data on the tail pipe emissions of four and two-wheeled vehicles. Data from 204 automobiles was taken into account. The results revealed that, even though BS-IV norms had been in force since 2010, the PUC certificate given by the transportation department had taken the BS-III emission limitations into account, failing just 2 petrol fuelled four-wheeler vehicles. Almost all motor cars complied with BS-III emission standards, while just around 9% of four-wheelers failed the BS - IV test limits. Furthermore, it was discovered that 18.51 percent of two-wheelers failed to fulfil the BS-VI emission standards for the selected pollutants (combined CO and HC). To assess the harm to human health posed by these tail pipe emissions, more investigation is needed.

**Keywords**

Air Pollution; Bharat Stage – IV and VI; Emission Norms

Received: 12 Mar 2023 | Accepted: 29 Aug 2023 | Online: 28 Sep 2023

**Cite this article**

Harshit Verma, Dipteek Parmar and Rajiv Ganguly (2023), Compliance of Vehicular Emission Norms in Kanpur City, India. *Engineering Research Transcripts*, 3, 33–40.

DOI: https://doi.org/10.55084/grinrey/ERT/978-81-964105-0-6_4

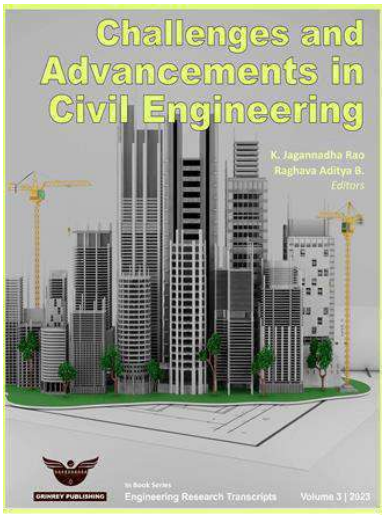

## 1. Introduction

The number of automobiles using the roads has increased significantly due to the growth in the urban population and the improvement in living standards. With average particulate matter concentrations 10 times higher than WHO limits, India is currently the fifth most polluted nation in the world [1]. In addition to negatively affecting human health, air pollution also negatively affects the nation's economy. A loss of $95 billion, or roughly 3% of the nation's GDP, happened in 2019 as a result of air pollution, and around 1.6 million fatalities per year are attributed to exposure to air pollutants [2] and [3]. Motorised vehicles are always needed for both private and public transportation as cities grow in size and population. Every year, some 25 million new cars are added to the country's roadways [4] [5]. This together with current vehicles make up a sizable source of air pollution. Around 22% of the world's greenhouse gas emissions are attributable to the transport sector alone, with road transport alone responsible for 70% of those emissions [6].

Automobiles are one of the main sources of air pollution because of the toxic exhaust fumes they produce. Spark ignition (SI) engines contribute to more oxides of carbon (CO and $CO_2$), hydrocarbons (HC), particulates (PM), and oxides of nitrogen ($NO_x$) than compression ignition (CI) engines. Diesel engines release relatively high levels of nitrogen dioxide ($NO_2$), but direct injection petrol engines emit very little of it [7].

The government has implemented a number of measures and programmes designed to improve air quality. Air Quality management includes monitoring the quality of the air. The National Air Monitoring Programme (NAMP) was established with the objectives of assessing the current condition and trends of air quality as well as managing and regulating pollution from industries and other sources. The pollution under control (PUC) programme was further established in India so as to regulate and manage automobile emissions. This programme attempts to maintain vehicle emissions below a predetermined threshold established up in accordance with Bharat Stage (BS) guidelines.

### 1.1 History of Emission Norms in India

India adopted the Air (Prevention and Control of Pollution) Act in 1981 to help minimize air pollution. It established the government with the power to regulate vehicle emission standards. The Motor Vehicles Act of 1989 assigned responsibility for creating and implementing vehicle emission standards to the Ministry of Road Transport and Highways (MoRTH) [8]. Following this, idle emission limitations were the first emission rules to be implemented in the nation in 1989. Mass emission restrictions, which went into effect in 1991 for gasoline-powered cars and 1992 for diesel-powered vehicles, swiftly replaced these standards. In April 1995, it became necessary for new petrol-powered passenger automobiles in four major cities—Delhi, Mumbai, Kolkata, and Chennai—to have catalytic converters installed. Beginning in 2000, India began adhering to the Bharat Stage (BS) emission requirements, which were similar to the EURO standards. The nationwide introduction of the Bharat stage I (BS-I) standards, which were comparable to the EURO- 1 standards, took place in 2000. Bharat Stage II regulations implementation began in 2001 and lasted through 2005 in various phases, encompassing various cities in various stages. The implementation schedule for the Bharat Stage requirements was outlined in the auto fuel policy, which was established in 2003. From 2005 to 2010, the BS-III rules were similarly applied in two parts. BS-IV standards were first introduced in a small number of places in 2010, and then they were expanded in 2015 and 2016 before being enforced nationwide in 2017. The BS - VI rules, which were correlated with the EURO - 6 requirements, were enacted and put into national effect in 2020 as a result of the BS - IV standards' delayed enforcement, which caused a discrepancy between them and the EURO emission standards. The criteria for the EURO emission

standards were not used in the creation of the emission limits for two and three-wheeled vehicles and these norms were prepared separately. [7][8][10].

**Table 1.** The development of India's emission regulations. [9]

| Standard | Year | Cities of Implementation |
|---|---|---|
| BS – I | 2000 | Countrywide |
| BS – II | 2001 | NCR#, Mumbai, Kolkata, Chennai |
| BS - II | 2003 | NCR#, 10 cities$ |
| BS – II | 2005 | Countrywide |
| BS – III | 2005 | NCR#, 10 cities$ |
| BS – III | 2010 | Nationwide |
| BS – IV | 2010 | NCR*, 12 cities^ |
| BS – IV | 2014 | 8 more cities in addition to the existing 12 cities, mainly in Northern India |
| BS – IV | 2017 | Countrywide |
| BS – V | - | Skipped |
| BS – VI | 2020 | Nationwide |

National Capital Region (NCR i.e., Delhi) is denoted by the sign #, Kanpur, Mumbai, Agra, Bangalore, Kolkata, Hyderabad, Pune, Surat, Chennai and Ahmedabad, are denoted by the symbol $, and Solapur and Lucknow are denoted by the symbol ^.

### 1.2 India's Current Vehicle Emission Regulation

India now adheres to Bharat Stage-VI emission standards. The limits for emissions of category M and N vehicles (GVW 3.5 Tonnes) that are powered by petrol or diesel are listed in Tables 2 and 3 [11].

In India, a certification programme called Pollution Under Control (PUC) was established in 2005. The PUC certificate requirements were taken from the Bharat Stage standards. Vehicles in India are legally required to get this certification.

**Table 2:** Four-wheeler category M and N vehicle emissions standards for petrol [11]

| Emission Norm | HC | CO | $NO_x$ | PM |
|---|---|---|---|---|
| BS – IV | 0.10 | 1.0 | 0.08 | None |
| BS – IV | 0.10 | 1.0 | 0.06 | 0.0045 |

**Table 3:** Four-wheeler category M and N vehicle emissions standards for diesel [11]

| Emission Norm | HC | CO | $NO_x$ | HC + $NO_x$ | PM |
|---|---|---|---|---|---|
| BS – IV | None | 0.50 | 0.25 | 0.30 | 0.025 |
| BS – IV | None | 0.50 | 0.06 | 0.170 | 0.0045 |

*All values are in gm/km

For gasoline-powered automobiles, idle CO and HC measurements are taken, whereas measures of free-acceleration smoke are taken for diesel-powered vehicles. The PUC program's establishment and administration are shared by both the national and state governments. The Central Ministry of Road Transport and Highways (MoRTH) and the Central Pollution and Control Board (CPCB) are in charge of specifying the testing methodologies, instruments, and emission restrictions. Table 4 illustrates the requirements for two- and four-wheeled vehicles to receive a PUC certificate as stated by the MoRTH [12].

**Table 4:** Vehicular Emission Standards for obtaining a PUC certificate for petrol powered vehicles [12]

| Emission Criteria | Four-Wheeler | | Two-Wheeler | |
|---|---|---|---|---|
| | CO (%) | HC (ppm) | CO (%) | HC (ppm) |
| BS – IV | 0.3 | 200 | 3.5 | 4500 |
| BS – IV | 0.3 | 200 | 0.5 | 500 |

## 2. Methodology

### 2.1 Study Area

In the north central area of the country, the city of Kanpur is located on the banks of the river Ganga. It is located in the Indo Gangetic Plain (IGP), which is among the most polluted areas in the globe due to its dense population and geographic conditions. With a population of about 45.81 lakh, Kanpur ranks as India's 12th-largest city [13]. Private motor vehicles, including both two- and four-wheelers, are the primary mode of mobility in the city.

### 2.2 Data Collection

The Kumar et al. (2018) study provided the secondary data that was utilized in this investigation. At the IOCL gas station on Benajhabar Road in Kanpur, emission data from 130 two-wheelers and 74 four-wheelers consisting of CO concentrations in percentage by volume and HC concentrations in parts per million were measured and recorded from January to April 2018. This information was gathered for automobiles that came at the gas station to get their PUC certificates. The emissions from the vehicle's tailpipes were monitored for pollution while they were idling. The constant volume sampling (CVS) method with continuous dilution was adopted for measuring the exhaust emissions. Non – Dispersive Infrared (NDIR) absorption analyzers were used to measure the CO emissions while Flame Ionization (FID) analyzers were adopted for HC measurement. Only gasoline-powered automobiles were used to assess the standards' compliance.

### 2.3 Computational Work

Simple analysis was performed on the received vehicular emission data for 130 two-wheelers and 74 four-wheelers, which included evaluating whether the data collected complied with both the PUC certificate

standards as well as BS-IV (2010) and BS-VI (2020) criteria. Correlation between the CO and HC measurements for all the vehicles and the correlation between the vehicle age and the pollutants considered was also calculated to determine whether the pollutants (CO and HC) emitted from the vehicles depend on each other and to also find out whether the age of the vehicles plays any role in the amount of pollutants emitted.

## 3. Results and Discussions

The findings of the vehicles compliance with the emission standards are shown in Table 5. It displays the quantity of automobiles that don't meet the different emission standards. The 130 two-wheelers that were tested all passed the BS-IV and the PUC emission standards, which suggests that the PUC and BS-IV standards that were in place at the time were not very strict. If BS-VI requirements are used, it is found that up to 81 and 29 motor vehicles, respectively, do not meet the emission norms for CO and HC. Additionally, out of 130 motorbikes, a total of 25 weren't compliant with both the CO and HC emission standards. In the case of four wheelers, 26 automobiles did not meet the CO limits, 3 cars did not meet the HC requirements, and 2 cars did not meet the PUC rules for both CO and HC. When the BS-IV rules were used, a total of 7 automobiles failed both test parameters, whereas 37 vehicles failed the CO limits and 8 vehicles failed the HC norms. Because four-wheelers are subject to the same BS-IV and BS-VI requirements for CO and HC, the number of failed vehicles remains constant.

For two-wheelers, the average CO and HC emissions are 0.84% and 390.02ppm, respectively, while for four-wheelers, the averages are 0.45% and 87.68 ppm, respectively. Weak correlation ($0.20 < r < 0.40$) was found between the age of the vehicle and the pollutants emitted from the vehicles. This was observed for both two and four wheelers, with a slightly better correlation observed for four wheeled vehicles. This represents that although there exists a association between the vehicle age and the emissions, there are other factors which also contribute to the amount of pollutants emitted. When observing the dependence of CO and HC on each other, moderate correlation ($0.40 < r < 0.60$) was found for two wheelers whereas weak correlation was found for four wheelers. This shows that for two wheelers the failure of emissions is concurrent whereas for four wheelers it occurs in different stages, implying that two wheelers pose a greater potential for pollution when compared to four wheelers. The correlation values are represented in table 6.

According to the data, a sizable fraction of both two-wheeler and four-wheeler vehicles do not adhere either to the CO emission standards, or the HC rules. Four-wheeled vehicles have a failure rate for CO emissions that is five times higher than that of the emission standards, while for two-wheeled vehicles, the failure rate for CO emissions is three times higher than the emission guidelines. This might be because of the result of inadequate fuel combustion in the engine, poor vehicle maintenance, or an engine with a richer fuel to air mixture. The percentage of automobiles failing both the independent and combined emission tests is shown in Figure 1 and 2.

**Table 5:** The total number of vehicles not complying with the emission standards

| Emission Rules | Four-Wheeler (out of 74) | | | Two-Wheeler (out of 130) | | |
|---|---|---|---|---|---|---|
| | Total | CO | HC | Total | CO | HC |
| As per PUC | 2 | 26 | 3 | 0 | 0 | 0 |
| BS – IV | 7 | 37 | 8 | 0 | 0 | 0 |
| BS – VI | 7 | 37 | 8 | 25 | 81 | 29 |

**Table 6:** Coefficient of Correlation of CO and HC emissions with vehicle age and with each other

| Type of Vehicle | Vehicle Age | | With each other |
|---|---|---|---|
| | With CO | With HC | |
| **Two-Wheeler** | 0.192 | 0.162 | 0.401 |
| **Four-Wheeler** | 0.217 | 0.250 | 0.320 |

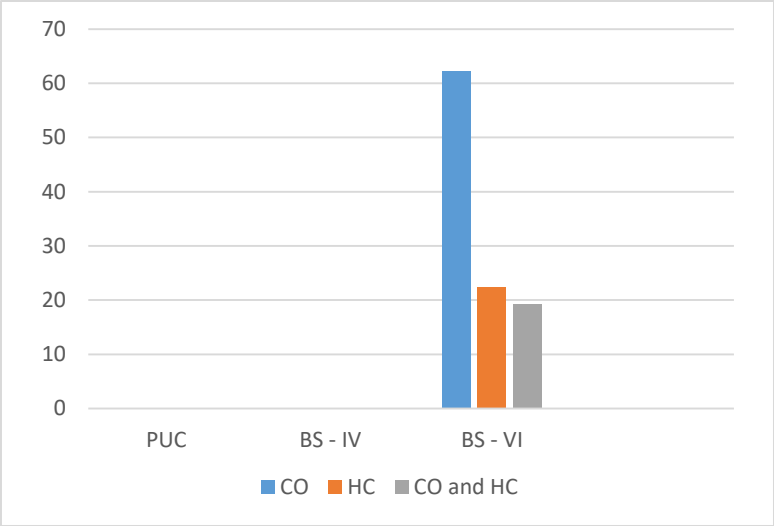


**Fig. 1.** Bar Chart representing the number of two wheelers failing the emission standards – PUC, BS – IV and BS - VI

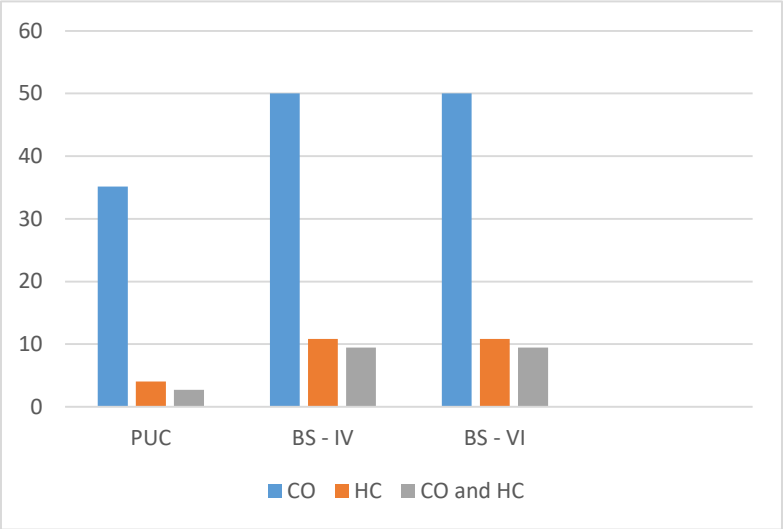


**Fig. 2.** Bar Chart representing the four wheeled vehicles failing the emission standards – PUC, BS -IV and BS – VI

## 4. Conclusion

According to the data collected for both two- and four-wheeler vehicles, the majority of two-wheeler motor vehicles meet PUC emission regulations, but when Bharat stage emission rules are applied, roughly 19% of the vehicles fail in the emission limits. Similarly, when PUC rules are used instead of Bharat stage

norms, just 2.5% of four-wheeler vehicles fail, compared to around 9% of cars under Bharat stage criteria. Despite the fact that four-wheelers were subject to BS-IV regulations in 2018, the PUC standards adhered to BS-III standards, which allowed for the certification of more vehicles. Furthermore, it has been discovered that automobiles break CO emission laws more frequently than HC regulations.

Further studies are required to be conducted on a larger sample pool, so as to account for the different vehicle classifications based on the type of fuel and size and mass category, and to also analyse the numerous different pollutants to be monitored. Future studies can also examine how these exhaust emissions affect the health of those who use the roads and work in the auto industry.

## Nomenclature

| | | |
|---|---|---|
| *mg* | : | Milligram |
| *km* | : | Kilometer |
| *ppm* | : | Particle per Million |
| *BS* | : | *Bharat Stage* |
| *CI* | : | *Compression Engine* |
| *CO* | : | *Carbon Monoxide* |
| *CPCB* | : | *Central Pollution Control Board* |
| *CVS* | : | *Constant Volume Sampling* |
| *EURO* | : | *European* |
| *FID* | : | *Flame Ionization Detector* |
| *GDP* | : | *Gross Domestic Product* |
| *GVW* | : | *Gross Vehicle Weight* |
| *HC* | : | *Hydrocarbon* |
| *IGP* | : | *Indo Gangetic Plain* |
| *MoRTH* | : | *Central Ministry of Road Transport and Highways* |
| *NAMP* | : | *National Air Monitoring Programme* |
| *NDIR* | : | *Non-Dispersive Infrared* |
| $NO_x$ | : | *Oxides of Nitrogen* |
| $NO_2$ | : | *Nitrogen Oxide* |
| *PM* | : | *Particulate Matter* |
| *PUC* | : | *Pollution Under Control* |
| *SI* | : | *Spark Ignition* |

## References

[1] World Air Quality Report Region and City PM2.5 Ranking, 2021. Retrieved from: https://www.iqair.com/world-most-polluted-cities/world-air-quality-report-2021-en.pdf Accessed 24 September 2022.

[2] Health Effects Institute. State of Global Air 2020 Special report on global exposure to air pollution and its health impacts, 2020. Retrieved from: https://www.stateofglobalair.org/ Accessed 13 October 2022.

[3] Gupta G., Singh A., Damani S., Bhatnagar R., Goyal S. and Biyani G. Air Pollution and its Impact on Businesses: The Silent Pandemic, 2021. Retrieved from: https://www.cleanairfund.org/resource/air-pollution-in-india-and-the-impact-on-business/ Accessed 05 October 2022.

[4] Road Transport Yearbook 2018 – 2019, 2021. Retrieved from: https://morth.nic.in/print/road-transport-year-books Accessed 17 October 2022.
[5] FADA: FY 2020-2021 Vehicle Registration data, 2021. Retrieved from: https://fada.in/press-release-list.php?page=2 Accessed date 19 October 2022.
[6] Jean-Paul Rodrigue. The Geography of Transportation Systems. 5th Edition. London: Routledge; 2020.
[7] Elavarasan G., Kannan M. and Karthikeyan D. History of Emission standards in India – A Critical review. International Journal of Research and Analytical Reviews. 2019; 6 (2), 28 – 35.
[8] [8] Singh S., Kulshrestha M. J., Rani N., Kumar K., Sharma C., and Aswal D. K. An Overview of Vehicular Emission Standards. 2022, MAPAN: Journal of Metrology Society of India. DOI: https://doi.org/10.1007/s12647-022-00555-4
[9] India Bharat Stage VI Emission Standards: Policy Updates. The International Council on Clean Transportation, 2016. Retrieved from: https://theicct.org/publication/india-bharat-stage-vi-emission-standards/ Accessed 22 October 2022.
[10] Vehicular Emission Norms, Ministry of Road Transport and Highways. Retrieved from: https://morth.nic.in/vehicular-emission-norms Accessed 18 October 2022.
[11] Indian Emission Regulation Booklet, The Automotive Research Association of India (ARIA), 2021.
[12] Central Motor Vehicle Rules, 1989. Ministry of Road Transport and Highways. Retrieved from: https://morth.nic.in/central-motor-vehicles-rules-1989-1 Accessed 13 October 2022.
[13] Census of India: Kanpur Nagar, 2011. Retrieved from: https://kanpurnagar.nic.in/demography/ Accessed 28 October 2022.

5

# Dynamic Analysis of Multiple Fire Domino Effects for Better Environmental Safety and Health Management

**Anagha Raveendran*, V R Renjith and G Madhu**

Cochin University of Science and Technology, Kochi, Kerala, India

*anagharavi94@gmail.com

## Abstract

Fire is a major hazard which frequently occurs in any flammable chemical processing industry leading to severe injuries, fatalities and environmental pollution. Fire induced domino accidents are of serious concern since its escalation to multiple target equipment results in more severe multiple fire scenario. Such multiple fire scenario in industrial clusters located at densely populated environment is a major threat to health and safety of human. Dynamic analysis of multiple fire domino effects is significant since the time to failure and start of fire at each equipment occurs at different times. A quantitative analysis of the dynamic variation in time to failure and failure probabilities of storage tanks during multiple fire domino effects is done. The concept of critical thermal dose is applied in this study for the estimation of dynamic time to failure of each vulnerable storage tank considering maximum synergistic effects based on the temporal variation in the intensity of heat radiation received by them. Improved probit equations are utilised for the calculation of failure probabilities of vulnerable storage tanks as a function of dynamic time to failure. The obtained results enhance timely implementation of accident mitigation measures to reduce associated health, safety and environment issues.

**Keywords**
Critical Thermal Dose, Domino Accident Analysis, Environmental Safety and Health, Multiple Fire Scenario

Received: 24 Mar 2023 | Accepted: 12 Sep 2023 | Online: 28 Sep 2023

**Cite this article**

Anagha Raveendran, V R Renjith and G Madhu (2023). Dynamic Analysis of Multiple Fire Domino Effects for Better Environmental Safety and Health Management. *Engineering Research Transcripts*, 3, 41–50.

DOI: https://doi.org/10.55084/grinrey/ERT/978-81-964105-0-6_5

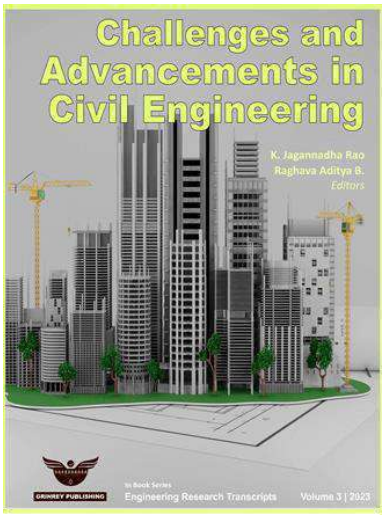

## 1. Introduction

Fire and explosion are major primary accidents in any flammable chemical storage tank facilities which result in catastrophic domino accidents by escalating towards nearby vulnerable storage tanks due to escalation vectors like heat radiation or overpressure [1]. Fire induced domino accidents are of serious concern in any hazardous chemical process industry. The prolonged duration of primary fires enhances its escalation to multiple target equipment to result in more severe multiple fire scenario [2]. Domino effects involving multiple fires are a major threat to environmental safety and health of people as it involves multiple heat radiation sources. This leads to severe injuries, fatalities and environmental pollution due to the production of irritating, corrosive and toxic gases along with heat radiation. Domino accidents are time-dependent processes. In case of multiple fire related domino effects, the intensity of heat radiation incident on a vulnerable unit and its time to failure (ttf) varies with time. The intensity of thermal radiation emitted and incident on a chemical storage tank depends on the tank diameter, burning rate of the chemical released, flame height etc. As stated in [3] and [4], once the intensity of heat radiation incident on a vulnerable equipment is greater than or equal to the damage/escalation threshold, the accident escalates to result in further domino accidents which are more severe than the initiating event i.e.; fire/explosion. The escalation of an accident through heat radiation from pool fire or tank fire is time-dependent which takes about a few minutes or even hours to cause damage to nearby storage units [2]. Thus, the time to failure /damage and consequent start of fire in each storage tank varies temporally especially during multiple fire domino accidents.

In this work, the concept of critical thermal dose is used to estimate dynamic ttf of vulnerable equipment according to temporal evolution of multiple fire scenario and temporal variation in the intensity of heat radiation received by it [5]. Improved probit equations are used to calculate failure probabilities of storage tanks incorporating the temporal variation in the thermal radiation incident on a vulnerable storage tank and its dynamic time to failure. The dynamic analysis of domino effects involving multiple radiation sources during a multiple fire scenario is significant for the estimation of dynamic time to failure and failure probabilities since the failure and start of fire at each at each storage tank occurs at different times. The estimation of dynamic time to failure of vulnerable storge tanks plays a major role in realistic implementation of accident escalation mitigation and protective measures to reduce health, safety and environmental issues. It also helps in realistic scheduling of emergency shutdown and fire control operations.

Among the following sections Section 2 defines the case study area and methodology used in this work. Section 3 provides various results along with a brief discussion on the major observations and output. Section 4 briefly conclude the significance of dynamic analysis of multiple fire domino effects for better health, safety and environment management.

## 2. Methodology

### 2.1 Study Area

In the present study, a Benzene storage tank farm from a petrochemical industry in South Asia. It is located at a densely populated industrial cluster with a potential for multiple fire domino effects leading to health, safety and environmental issues is selected. It consists of 8 storage tanks of Benzene at atmospheric condition as shown in the google earth image in Figure.1. Schematic representation of storage tanks is given in Figure. 2. Diameter (m) and total volume ($m^3$) of each tank are given in Table. 1.


**Fig. 1.** Google Earth image of the Benzene storage tank farm (Courtesy: Google Earth)

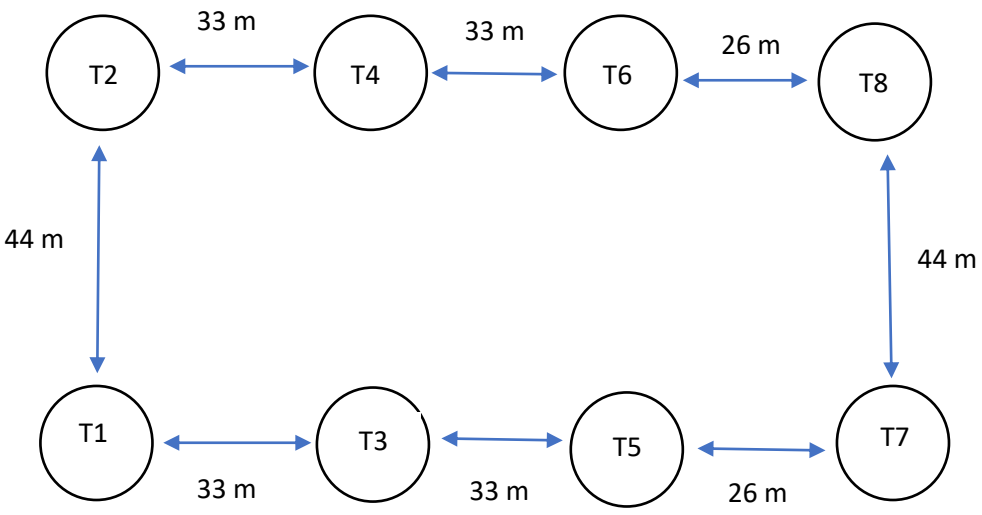


**Fig. 2.** Schematic representation of centre-to-centre distance between storage tanks

**Table 1.** Diameter and Volume of Storage Tanks

| Tank Name | Diameter (m) | Volume ($m^3$) |
|---|---|---|
| T1 | 14 | 1000 |
| T2 | 21 | 3300 |
| T3 | 14 | 1000 |
| T4 | 21 | 3000 |
| T5 | 21 | 3000 |
| T6 | 21 | 3000 |
| T7 | 10.5 | 690 |
| T8 | 10.5 | 690 |

### 2.2 Dynamic Time to Failure

In case of fire related domino effects, the heat radiation from multiple fires; especially at higher order domino effects, causes synergistic effects which increases the failure probability of a vulnerable storage tank [5]. Many researchers adopted the probit equations indicated in [6] and [7] for the calculation of damage probability of a vulnerable equipment. However, these probit equations do not consider dynamic ttf. In this study, we used improved probit equations (1) and (2) for the calculation of escalation/damage probability of a vulnerable equipment by considering its dynamic ttf [5]:

For all heat radiation scenarios:

$$Y = 9.25 - 1.85\ln(ttf)\,;\ ttf\ (min) \tag{1}$$

$$\ln(ttf) = -1.128\ln(I) - 2.667 \times 10^{-5}V + 9.877;\ ttf\ in\ seconds \tag{2}$$

$P_0$ denotes intensity of overpressure (Pa), ttf is time to failure, V is volume of storage tank ($m^3$) and I is intensity of heat radiation (9 $kW/m^2$).

The domino affected accident escalation/damage probability of a vulnerable equipment is estimated from the Standard Normal Cumulative Distribution Function *φ(Y-5)*, where Y is the probit value obtained from Equation (1).

The equations (3) to (8) are used for the calculation of dynamic ttf as a function of critical thermal dose $D_{th}$ [5]:

The critical thermal dose $D_{th}$ required to cause tank failure:

$$D_{th} = Q^{\alpha}\ \times ttf; ttf\ in\ seconds, \alpha \text{ is a constant} \tag{3}$$

For atmospheric equipment,

$$D_{th} = Q^{1.128} \times ttf = e^{-(2.667\times10^{-5}\times V - 9.877)};\ ttf\ (sec), V\ (m^3), Q\ (\frac{kW}{m^2}) \tag{4}$$

Q is the constant value of thermal radiation incident on the vulnerable equipment, V is the constant volume of vulnerable equipment. Q and ttf are inversely proportional.

While considering a time-dependent variation in the thermal radiation incident on the vulnerable storage tank,

$$D_{th} = \int_0^{ttf} Q^{\alpha} \times dt \tag{5}$$

During a stationary pool fire, the thermal radiation incident on a vulnerable storage tank is a step function which remains constant until a new fire occurs and changes temporally once a new fire occurs. Thus, the critical thermal dose can be simplified as:

$$D_{th} = \sum_{i=1}^{n} Q_{0,i}^{\alpha} . \Delta t_i \tag{6}$$

$Q_{0,i}^{\alpha}$ denotes the total heat radiation incident on a vulnerable equipment at each time interval, $\Delta t_i$ denotes the length of each time interval and n denotes the total number of time intervals.

A vulnerable storage tank fails at the end of $n^{th}$ time interval to start a fire. Thus, the dynamic ttf of a vulnerable storage tank, when the ttf of other tanks are known:

$$ttf = \sum_{i=1}^{n-1} \Delta t_i + \Delta t \tag{7}$$

Where,

$$\Delta t = \frac{D_{th} - \sum_{i=1}^{n-1} Q_{0,i}^{\alpha} . \ \Delta t_i}{Q_{0,n}^{\alpha}} \tag{8}$$

Dynamic ttf of a vulnerable equipment in (7) accounts for the effect of thermal radiation from multiple fires which initiate at different points of time [5]. The time-dependent estimation of ttf is more realistic as it maximizes synergistic effect during multiple fire scenario. Thus, it helps to implement a more realistic environmental safety and health protection measures. The damage threshold of the atmospheric units is taken as 15kW/m$^2$ [3], [4] and [8]. Mass burning rate and flame height during a pool fire are calculated for each tank the estimation of emitted and received heat radiation using classical empirical equations from TNO multi-energy models are well discussed in [9] and [10]. TNO is the Netherlands Organization for Applied Scientific Research.

The mass burning rate of a liquid is calculated as

$$\frac{dm}{dt} = \frac{0.001\, H_C}{C_p(T_b - T_a) + H_{vap}} \text{ When } T_b > T_a \tag{9}$$

And

$$\frac{dm}{dt} = \frac{0.001\, H_C}{H_{vap}} \quad \text{When } T_b < T_a \tag{10}$$

Where $T_a$ is the ambient temperature (K), $T_b$ is the boiling point (K) of the liquid, $H_C$ is the net heat of combustion (energy/mass), $H_{vap}$ is the heat of vaporization of the liquid at $T_a$, (energy/mass).

The total heat radiation emitted from a pool of radius 'r' is given as

$$Q = \frac{\left(\pi r^2 + 2\pi r H\right) . \left[\frac{dm}{dt}\right] . \eta\, H_C}{72 . \left[\frac{dm}{dt}\right]^{0.61} + 1} \tag{11}$$

η is the efficiency factor (0.13 to 0.35), H is the flame height (m)

$$H = 84\, r \left[\frac{\left(\frac{dm}{dt}\right)}{\rho_a\, (2gr)^{\frac{1}{2}}}\right]^{0.6} \tag{12}$$

$\rho_a$ is the air density (1.2 kg/m$^3$ at 20°C and 1 atm.) and $g$ is the acceleration of gravity (9.81 m/s$^2$).
The heat radiation received by a storage tank at a distance R from the centre of pool fire is,

$$I = \frac{TQ}{4\pi R^2} \tag{13}$$

T is the transmissivity of the air path (Approx. 1).

## 3. Results and Discussions

The vertical burning rate of Benzene is generally 6 mm/min or 0.0001 m/s as per the safety datasheet of Benzene. Further, the mass burning rate is calculated as 0.0876 kg/m$^2$s by multiplying the vertical burning rate with the density of benzene (876 kg/m$^3$). The flame height and emitted heat flux from each storage tank are obtained as shown in Table. 2.

**Table 2.** Flame Height and Emitted Heat Radiation of each storage tank

| Tank Name | Flame Height (m) | Emitted Heat Flux (kW/m$^2$) |
|---|---|---|
| T1 | 26.54 | 53721.9 |
| T2 | 35.19 | 108481 |
| T3 | 26.54 | 53721.9 |
| T4 | 35.19 | 108481 |
| T5 | 35.19 | 108481 |
| T6 | 35.19 | 108481 |
| T7 | 21.73 | 32666.4 |
| T8 | 21.73 | 32666.4 |

The intensity of thermal radiation incident on each storage tank estimated using classical empirical equations from TNO multi-energy models [9] and [10] are given in Table. 3.

**Table 3.** Intensity of Incident Thermal Radiation

| **Heat Radiation Incident on Each Target Tank (kW/m$^2$)** | | | | | | | | |
|---|---|---|---|---|---|---|---|---|
| | **T1** | **T2** | **T3** | **T4** | **T5** | **T6** | **T7** | **T8** |
| **T1** | X | 3.81 | 6.32 | 1.49 | 1.39 | 0.64 | 0.57 | 0.35 |
| **T2** | 6.31 | X | 6.31 | 17.05 | 3 | 2.80 | 1.33 | 1.15 |
| **T3** | 6.32 | 3.81 | X | 3.81 | 8.44 | 1.48 | 1.48 | 0.66 |
| **T4** | 2.64 | 17.05 | 6.3 | X | 7.7 | 17.05 | 2.99 | 2.99 |
| **T5** | 2.48 | 3 | 12.77 | 7.69 | X | 7.69 | 20.05 | 2.99 |
| **T6** | 1.19 | 2.8 | 2.64 | 17.05 | 7.69 | X | 6.43 | 20.05 |
| **T7** | 0.36 | 0.46 | 0.96 | 1.11 | 10.82 | 2.64 | X | 1.73 |
| **T8** | 0.22 | 0.39 | 0.42 | 1.105 | 1.11 | 10.82 | 1.73 | X |

From the values of heat radiation intensities given in Table. 3, it is identified that:

- The heat radiation from T1, T3, T7 and T8 did not exceed the escalation/damage threshold (15 kW/m$^2$) of any of the tanks.
- The thermal radiation incident on T4 from T2 was greater than the escalation/damage threshold (17.05 kW/m$^2$).
- The heat radiation incident from T4 was greater than the escalation/damage threshold (17.05 kW/m$^2$) of T2 and T6.
- T5 affected T7 by a thermal radiation of 20.05 kW/m$^2$.
- The heat radiation received by T4 (17.05 kW/m$^2$) and T8 (20.05 kW/m$^2$) from T6 exceeded the escalation/damage threshold.

According to the above observations, T2, T4, T5 and T6 are found to be critical storage tanks. It is to be noted that T4 and T6 affected more than one storage tank at a time. So, these tanks are considered as most critical storage tanks. However, in this study, T2 is chosen as the primary tank in which the fire is assumed to be initiated.

However, all the storage tanks except the primary tank T2, are preheated by the heat radiation below their damage threshold before receiving an overall heat radiation which exceeds their damage thresholds either from an individual source or through synergistic effects. This time dependent variation in the incident heat radiation necessitates the estimation dynamic ttf as a function of tank volume as well as critical thermal dose. Dynamic ttf of each vulnerable storage tank from the beginning of initial fire is utilised for the estimation of dynamic accident escalation probabilities using the improved probit models [5].

When T2, T4 and T6 are damaged consecutively, the overall thermal radiation incident on T3 (15.25 kW/m$^2$) exceeded the damage threshold to catch fire. Also, the overall thermal radiation incident on T5 (18.39 kW/m$^2$) exceeded the damage threshold to catch fire. The overall thermal radiation incident on T1 (16.46 kW/m$^2$) through the synergistic effects of T2, T3, T4 and T6 exceeded the damage threshold to catch fire. It is also identified that the damage of T3 is essential to cause the damage of T1 through synergistic effects. Table. 4. shows the ttf of vulnerable storage tanks from the beginning of initial fire calculated using the simple summative methods discussed in [6] and [7]. In simple summative method only the total sum of thermal radiation received by a target tank is considered while calculating ttf. This method does not consider the time dependent variation in the intensity of heat radiation received by a target tank from multiple fire sources. Table. 4. also shows the dynamic ttf of vulnerable tanks from the beginning of initial fire calculated using the concept of critical thermal dose [5].

**Table 4.** Dynamic ttf of storage tanks since the start of primary fire

| **Tank Name** | **Critical Thermal Dose $D_{th}$** | **Time to Failure (ttf) using direct summative method (min)** | **Dynamic Time to Failure using critical thermal dose (min)** |
|---|---|---|---|
| T1 | 18964.6 | 11.42 | 23.77 |
| T2 | 17836.26 | 0 | 0 |
| T3 | 18964.6 | 14.6 | 18.12 |
| T4 | 17979.5 | 12.22 | 2.48 |
| T5 | 17979.5 | 11.22 | 17.97 |
| T6 | 17979.5 | 10.29 | 12.5 |
| T7 | 19122 | 6.67 | 21.81 |
| T8 | 19122 | 8.76 | 19.8 |

In the direct summative method, the summation of the overall thermal radiation incident on the vulnerable storage tank is directly utilized for the calculation of time to failure by also considering the incident heat radiation preheating the tank. Dynamic time to failure is calculated utilizing the critical thermal dose as a function of overall thermal radiation incident on the vulnerable storage tank at each time interval. From the dynamic time to failure of T3 and T5 which are failed by the synergistic effects of T2, T4 and T6, it is identified that T5 fails before T3. Thus, in order to calculate the time to failure of T1, which is failed by the synergistic effects of T2, T3, T4 and T6, the preheating by T5 is also considered in the overall heat radiation. This reduced the time to failure of T1 from 13.42 min to 11.42 min.

The dynamic failure probabilities of each storage tank are calculated using the improved probit equations (1) and (2) by considering their dynamic time to failure obtained using (7). The dynamic failure probabilities of each storage tank through domino effects once the primary tank T2 catches fire are tabulated in Table 5.

**Table 5**. Dynamic failure probabilities of storage tanks

| Tank Name | Dynamic Failure Probabilities |
|---|---|
| T1 | 0.054 |
| T2 | Primary Tank |
| T3 | 0.134 |
| T4 | 0.995 |
| T5 | 0.137 |
| T6 | 0.337 |
| T7 | 0.0735 |
| T8 | 0.054 |

From Tables 4 and 5, it is evident that higher the dynamic ttf, lower is the dynamic failure probability. Comparatively, higher failure probability implies higher possibility to fail.

## 4. Conclusions

Dynamic time to failure of each vulnerable storage tank accounts for the effect of time dependent variation in the heat radiation received from multiple fires in storage tanks which fail and catch fire at different times. The concept of critical thermal dose and synergistic effects are utilised to calculate dynamic ttf. The time-dependent estimation of ttf is more realistic as it maximizes synergistic effects during a multiple fire scenario. The estimation of dynamic time to failure can be utilised to calculate dynamic failure probabilities of storage tanks during multiple fire domino effects. It is evident from this case study that higher the dynamic time to failure of a vulnerable equipment, lower is its dynamic failure probability. Higher the failure probability of a vulnerable equipment, higher is its possibility to fail. Preheating of storage tanks by heat radiation below their threshold limits significantly reduces their time to failure.

From the analysis of heat radiation intensity in Table 3, it is concluded that T2, T4, T5 and T6 are critical storage tanks. Since T4 and T6 impact more than one storage tank at a time, these two tanks are considered as the most critical storage tanks that needs to be isolated first. From Table 4, it is observed that dynamic ttf using the concept of critical thermal dose comparatively provided more realistic time dependent cumulative failure time. From the dynamic ttf, the sequential order of failure of storage tanks is identified as T2, T4, T6, T5, T3, T8, T7 and T1. The dynamic time to failure and dynamic failure probabilities of storage tanks helps to implement a more realistic scheduling of emergency shutdown, accident mitigation and protection activities during multiple fire domino effects through real-time health, safety and environmental management.

## References

[1] Necci A, Cozzani V, Spadoni G, Khan F, Assessment of domino effect: State of the art and research needs, Reliability Engineering System Safety. 143 (2015) 3–18. doi:10.1016/j.ress.2015.05.017.

[2] Huang K, Chen G, Khan F, Yang Y, Dynamic analysis for fire-induced domino effects in

chemical process industries, Process Safety and Environmental Protection. 148 (2021) 686–97. doi:10.1016/j.psep.2021.01.042.

[3] Cozzani V, Gubinelli G, Salzano E, Escalation thresholds in the assessment of domino accidental events, Journal of Hazardous Materials A129. 129 (2006) 1–21. doi:10.1016/j.jhazmat.2005.08.012.

[4] Cozzani V, Tugnoli A, Bonvicini S, Salzano E, Threshold-based approach, Domino Effects in the Process Industries. Modeling, Prevention and Managing, Elsevier, 2013, 189–207. doi:10.1016/B978-0-444-54323-3.00009-9.

[5] Zhou J, Reniers G, Cozzani V, Improved probit models to assess equipment failure caused by domino effect accounting for dynamic and synergistic effects of multiple fires, Process Safety and Environmental Protection. 154 (2021) 306–14. doi:10.1016/j.psep.2021.08.020.

[6] Cozzani V, Gubinelli G, Antonioni G, Spadoni G, Zanelli S, The assessment of risk caused by domino effect in quantitative area risk analysis, Journal of Hazardous Materials. 127 (2005) 14–30. doi:10.1016/j.jhazmat.2005.07.003.

[7] Landucci G, Gubinelli G, Antonioni G, Cozzani V, The assessment of the damage probability of storage tanks in domino events triggered by fire, Accident Analysis & Prevention. 41 (2009) 1206–15. doi:10.1016/j.aap.2008.05.006.

[8] Khakzad N, Khan F, Amyotte P, Cozzani V, Domino effect analysis using Bayesian networks, Risk Analysis. 33 (2013) 292–306. doi:10.1111/j.1539-6924.2012.01854.x.

[9] Technica L. Techniques for assessing industrial hazards. A manual, World Bank Technical Paper Number 55; 1988.

[10] CCPS. Guidelines for Chemical Process Quantitative Risk Analysis. Second Edi. American Institute of Chemical Engineers .

# 6 Development of a Robotic Complex for the Manufacture of Parts Used in Civil Engineering

**Olga Afanaseva*, Timur Tulyakov, Daniil Romashin and Anastasia Panova**

Department of System Analysis and Management, Saint Petersburg mining university, Saint Petersburg, Russia

* afanaseva_ov@pers.spmi.ru

## Abstract

The article proposes a methodology for the development of a robotic complex for the manufacture of building parts. An analysis was carried out to select the most preferable option for the layout of the robotic complex and the option was selected using the method of the resulting quality indicator, consisting of an industrial floor robot, a mechatronic lathe and a storage device. Requirements for the manufacture of parts using the SolidWorks computer-aided design system (finite element method). The optimal robotic device was selected using the hierarchy analysis method, which could perform tasks related to loading and unloading parts into the machine. Auxiliary equipment was selected for the safe operation of the robotic complex - sensors and protective columns that would meet the standards of modern production of parts. Graphic materials were developed for a ready-made robotic complex consisting of a floor robot, a mechatronic lathe and a storage device, taking into account safety precautions at the workplace.

**Keywords**

Computer-aided design system, layout of machine equipment, mechatronic machine equipment, robotic complex

Received: 14 Mar 2023 | Accepted: 20 Sep 2023 | Online: 28 Sep 2023

**Cite this article**

Olga Afanaseva, Timur Tulyakov, Daniil Romashin and Anastasia Panova (2023). Development of a Robotic Complex for the Manufacture of Parts Used in Civil Engineering. *Engineering Research Transcripts*, 3, 51–58.

DOI: https://doi.org/10.55084/grinrey/ERT/978-81-964105-0-6_6

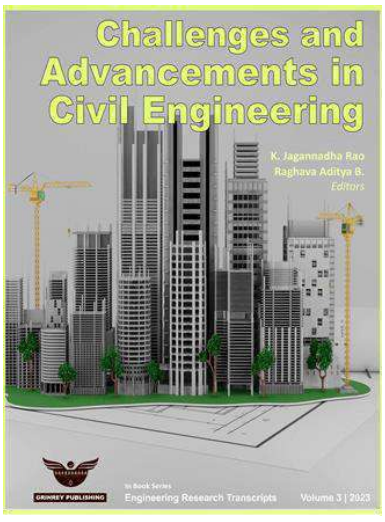

## 1. Introduction

The modern production of manufacturing parts for construction work must comply with the trends that set the following tasks: increasing productivity [6, 10, 12] [1-3], increasing the accuracy of processing, as well as expanding the functionality of technological equipment [5, 7, 13] [4-6] through the introduction of new technological solutions [4, 9, 14][7-9].

Modern construction cannot be imagined without the use of details [15, 17, 22][10-12]. These simple, at first glance, structural elements are indispensable in the construction of residential buildings, shopping and office centers, sports facilities, public buildings and workshops of industrial enterprises [18, 20, 21][13-15].

For quick and reliable delivery of the required parts used in construction, a modern solution for the manufacture of these parts [16, 19, 23][16-18] is required. That is why a methodology for the development of a robotic complex for the manufacture of building parts is proposed. This solution is the most reliable and efficient [24, 26][19-20].

The purpose of this work is to develop a robotic complex for the manufacture of parts used in the construction of various types of buildings and structures.

The initial stage in the course of introducing new technological equipment is the technical development of the proposal.

## 2. The Choice of the Layout of the Robotic Complex

This section describes the information about the structure of the article. The initial part of the manuscript should consist of a concise article title, name of the authors with **affiliation, abstract and keywords**. Further the manuscript text can be divided into different numbered sections such as,

To design a robotic complex, you must first choose its optimal layout using the method of the resulting quality indicator, namely the additive criterion. The essence of this criterion is to obtain the objective function by adding the normative values of particular criteria [3, 11, 25][21-23].

The calculation by this method using the Matlab system is shown in Fig. 1.

```
>> F=[0.53 4 4; 1.06 2 2]

F =

    0.5300    4.0000    4.0000
    1.0600    2.0000    2.0000

>> p1=0.5;
>> p2=0.4;
>> p3=0.6;
>> C1=p1*F(1,1)+p2*F(1,2)+p3*F(1,3)

C1 =

    4.2650

>> C2=p1*F(2,1)+p2*F(2,2)*p3*F(2,3)

C2 =

    1.4900

>> m=[C1 C2];
>> x=max(m)

x =

    4.2650
```

**Fig. 1.** Calculation of the layout of the robotic complex in Matlab

The program has chosen the value corresponding to the first variant of the layout of the robotic complex - a floor robot + 1 machine.

## 3. Choosing an Industrial Robot

To justify the choice of an industrial robot, we will use the Hierarchy Analysis Method (HAI) [27, 30, 33][24-26]. This method consists of building hierarchies, where at the top is the goal (in our case, an industrial robot), in the middle are the criteria for choosing a robot (E21-technical indicators, E22 - maintenance of the robot and E23 - economic indicators) and at the bottom level alternatives are presented to achieve the set targets (A1 – Eidos Robotics (ER) industrial robot, A2 – KUKA industrial robot, A3 – FANUC industrial robot). A notation is also introduced, where E are the evaluation criteria, A are alternatives for solving the set goal.

The hierarchy of industrial robot selection is shown in Fig. 2.

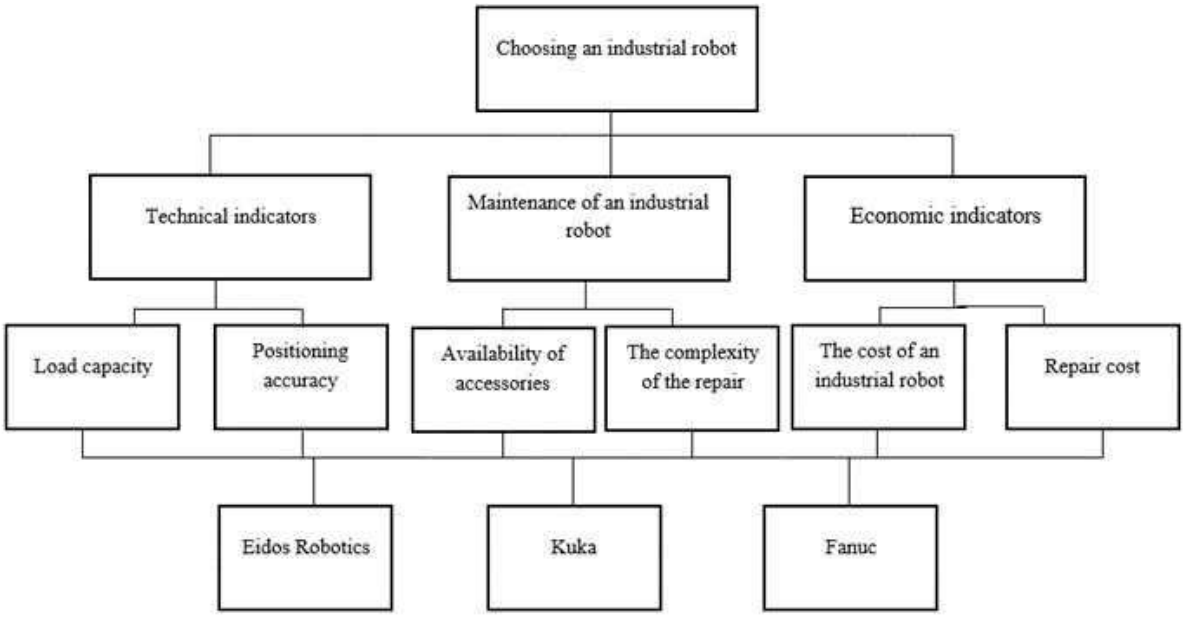


**Fig. 2.** Hierarchy of industrial robot selection

After the analysis, it can be concluded that the most preferable option is to choose an industrial robot from ER.

## 4. Choice of Machine Layout

Because for the manufacture of parts for construction, the executive movements of lathes and milling machines are required, then a lathe with the ability to perform milling model 200HTP is selected.

To improve the dynamic characteristics of the machine, it is required to analyze the possible layouts of the designed machine [1, 28, 29][27-29]. Possible layouts of the machine are selected according to the theory of Yu.D. Vragov and highlights possible workable options presented in Table 1.

**Table 1.** Machine layout options

| Considered layout | |
|---|---|
| cOXZ | cXZO |
| cOZX | cXOZ |
| cZOX | cZXO |

As you can see from tables 1, the most preferred options for machine layouts from a design point of view and the execution of the required executive movements are the layouts cOXZ and cZOX.

During the analysis, the SolidWorks Simulation program was used to solve problems by the finite element method (FEM). The finite element method is a grid method designed to solve micro-level problems,

for which the object model is given by a system of partial differential equations with given boundary conditions [2, 31, 32][30-32].

Comparing the results of studies of layouts according to the graphs (Fig. 3), we see that the rigidity of the second layout is higher than that of the first layout.

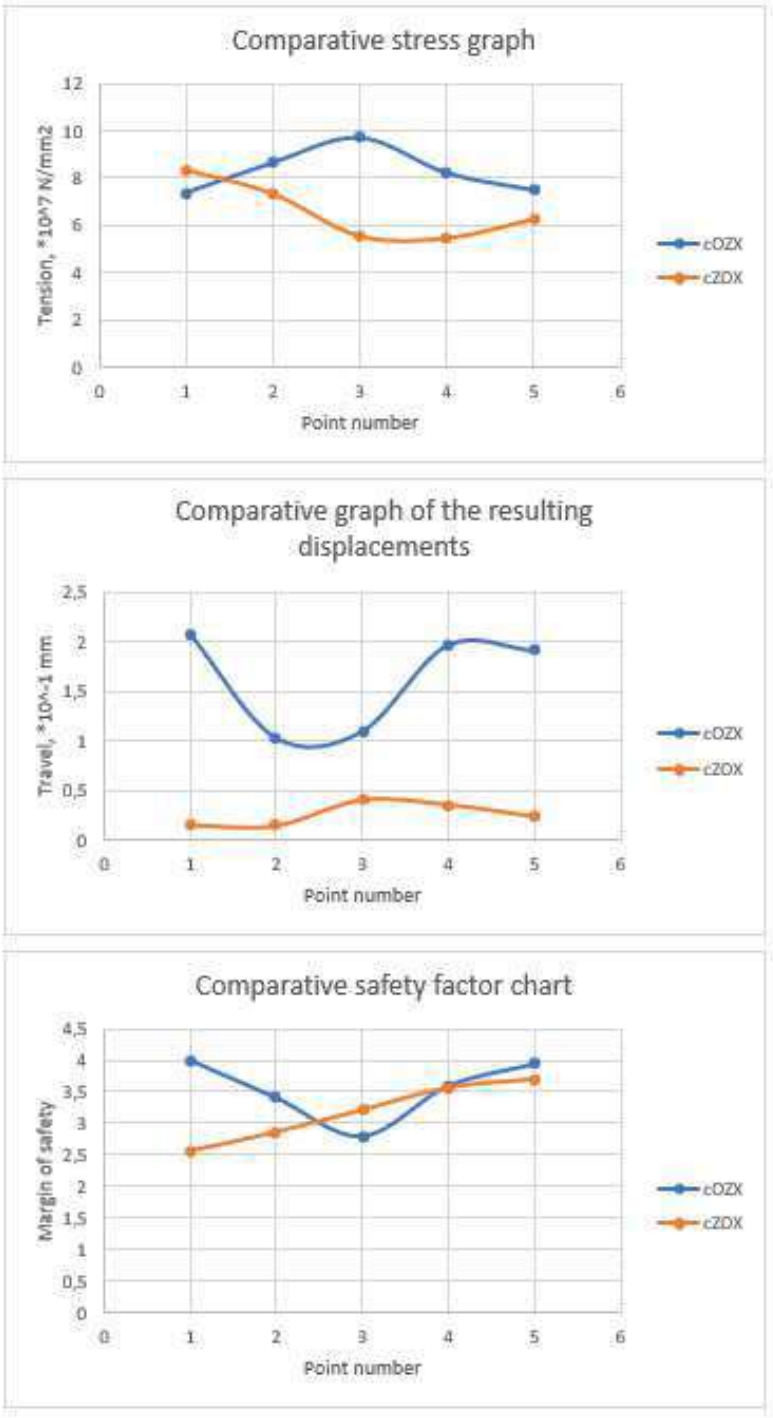


**Fig. 3.** Plots comparing cOZX and cZOX

We choose cZOX layout, since it is better in terms of static stiffness criteria and simpler from a constructive point of view.

## 5. The Choice of Sensors for the Safe Operation of the Robotic Complex

Instead of using protective barriers, the security of the robotic complex can be achieved with a simple combination of a pair of light curtains and mirror columns. The mirror columns reflect the beams of the light

curtains in such a way that one pair of light curtains is enough to control all three sides for access. This allows not only to provide access control to the hazardous area, but also to rationalize the use of space, reduce costs and installation time [8, 34, 35][33-35].

For the developed robotic complex, columns were chosen, located on 4 sides around the complex for positive protection and uninterrupted operation of the machine and robot.

## 6. Development of Design Documentation

The development of design documentation includes taking into account all the requirements for the operation of the robot and the machine, as well as taking into account safety requirements, because people are working nearby.

The developed documentation for the robotic complex, consisting of a machine tool, a floor robot and a storage device, is shown in Fig. 4.

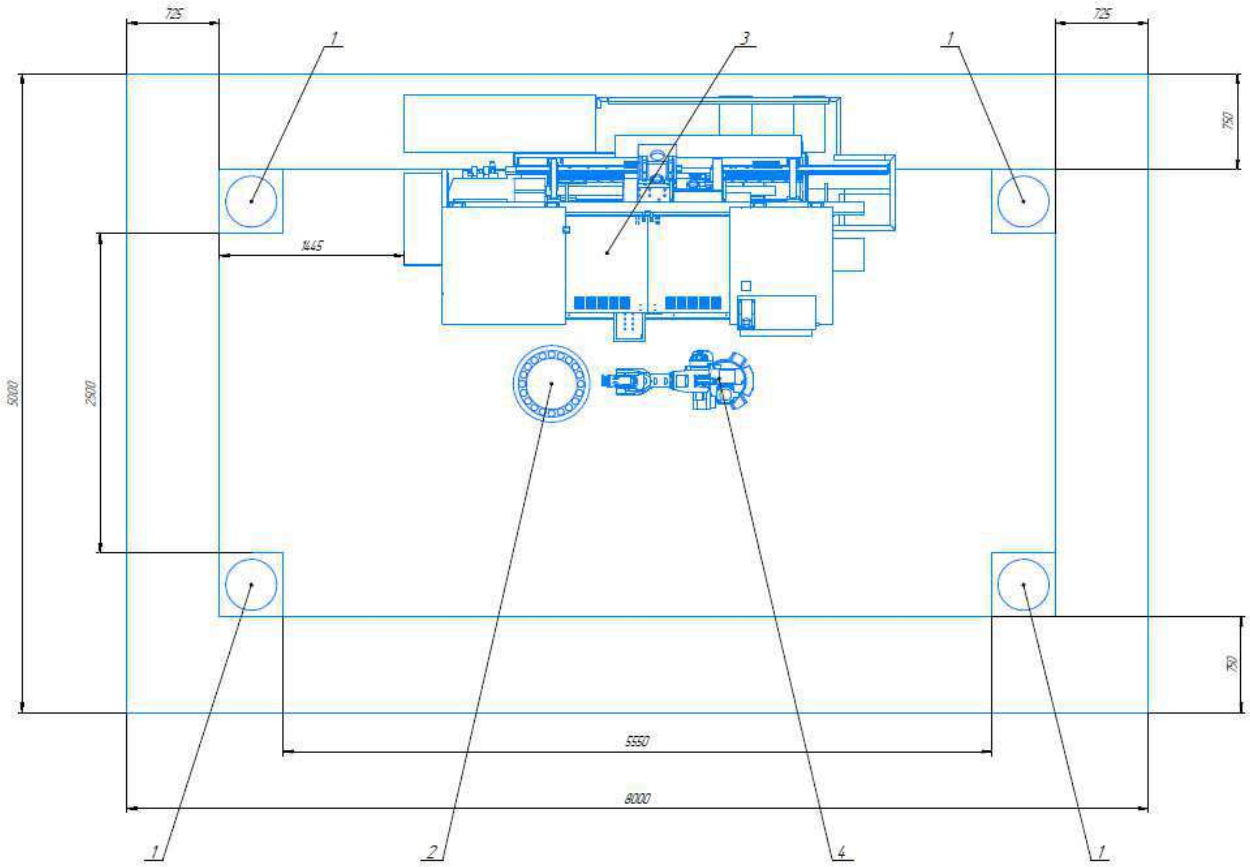


**Fig. 4.** Sketch of the layout of a robotic complex for the manufacture of parts for construction
1 - columns with sensors; 2 - storage device; 3 - machine; 4 - industrial robot

This design solution reflects all modern trends in the manufacture of parts not only in the construction area, but also in adjacent areas.

## 7. Conclusion

In the course of this work, a robotic complex was developed for the manufacture of parts for the construction industry.

The optimal robotic device for unloading and loading parts into the machine was selected, which is a floor-standing industrial robot.

A machine was selected from a variety of different layouts that would satisfy the requirements for the manufacture of building parts, and with the help of the CAE system and the finite element method, the optimal layout of mechatronic machine tool equipment was selected - cZOX

The security sensors of the robotic complex were selected, which with 100% probability would allow the complex to work without failures due to the human factor.

Design documentation for the robotic complex was developed, based on the previously selected layout of the robotic complex, consisting of a floor robot, a machine tool and a storage device, which took into account all the operational properties and safety standards of the designed complex.

## References

[1] S. V. Razmanova, O. V. Andrukhova. Oilfield service companies as part of economy digitalization: Assessment of the prospects for innovative development. Journal of Mining Institute. 2020; 244(4): 482–492. DOI: 10.31897/PMI.2020.4.11.

[2] D. Zakaev, L. Nikolaichuk., F. Irina. Problems of oil refining industry development in Russia. International Journal of Engineering Research and Technology. 2020; 13 (2): 267-270.

[3] K. D. Krestovnikov, E. O. Cherskikh, A. V. Saveliev. Investigation of the influence of the length of the intermediate magnetic circuit on the characteristics of magnetic gripper for robotic complexes of the mining industry. Journal of Mining Institute. 2020; Vol.241: 46. DOI: 10.31897/pmi.2020.1.46.

[4] V.V. Yurak, A. V. Dushin, L. A. Mochalova. Vs sustainable development: scenarios for the future. Journal of Mining Institute. 2020; Vol 242: 242. DOI: 10.31897/pmi.2020.2.242

[5] M. P. Afanasyev. Simulation of the Centrifugal Compressor Flow Part of the Internal Combustion Engine to Determine Areas of Non-Evaporated Moisture Effective Discharge during Charge Air Evaporative Cooling. IOP Conference Series: Earth and Environmental Science. 2020; 459 (2),: 022053. DOI: 10.1088/1755-1315/459/2/022053.

[6] A. S. Vasil'ev, A. A. Goncharov. Special strategy of treatment of difficulty-profile conical screw surfaces of single-screw compressors working bodies. Journal of Mining Institute. 2019; Vol.235: 60. DOI: 10.31897/pmi.2019.1.60.

[7] P. M. Afanasev. Simulation of Liquid Fuel Spills Combustion Dynamics Based on Computational Fluid Dynamics Using Modern Application Programs. IOP Conference Series: Earth and Environmental Science. 2020; 459 (2): 022034. DOI: 10.1088/1755-1315/459/2/022034.

[8] I. B. Movchan,A. A. Yakovleva. Refined assessment of seismic microzonation with a priori data optimisation. Journal of Mining Institute. 2019; Vol.236: 133. DOI: 10.31897/pmi.2019.2.133

[9] A. V. Martirosyan, Y. V. Ilyushin. Modeling of the Natural Objects Temperature Field Distribution Using a Supercomputer. Informatics. 2022; 9 (3): 62. DOI: 10.3390/informatics9030062

[10] V. V. Maksarov, A. I. Keksin, I. A. Filipenko. Influence of magnetic-abrasive processing on roughness of flat products made of amts grade aluminum alloy. Tsvetnye Metally. 2022; Vol.7: 82-87. DOI: 10.17580/tsm.2022.07.09.

[11] V. V. Gabov, D. A. Zadkov, A. Y. Kuzkin, A. S. Elikhin. Fractured-Laminar Structure of Formations and Methods of Coal Loosening Key. Engineering Materials. 2020; Vol.836: 90-96. DOI: 10.4028/www.scientific.net/KEM.836.90.

[12] J. F. Mammadov, B. Valiyeva, A. S. gizi Huseynova, and Y. M. gizi Hasanova. Development of diagnostic subsystem for manufacturing active elements in instrument-making industry. Vestnik of Astrakhan State Technical University. Series: Management, computer science and informatics. 2022; Vol.2022: 16-21. DOI: 10.24143/2073-5529-2022-1-16-21.

[13] N. Yu. Motyakov, D. R. Iakupov, P. V. Ivanova, S. L. Ivanov. Bucket positioning and its load content during mining in inundated mineral deposit. E3S Web of Conferences. 2021; Vol.326: 1-5. DOI: 10.1051/e3sconf/202132600003.

[14] L. Yuan. Fabrication of metallic parts with overhanging structures using the robotic wire arc additive manufacturing. Journal of Manufacturing Processes. 2021; Vol.63: 24-34. DOI: 10.1016/J.JMAPRO.2020.03.018.

[15] M. Blatnický, J. Dižo, J. Gerlici, M. Sága, T. Lack, and E. Kuba. Design of a robotic manipulator for handling products of automotive industry. International Journal of Advanced Robotic Systems. 2020; Vol.17: 172988142090629. DOI: 10.1177/1729881420906290.

[16] D. A. Zadkov, V. V. Gabov, N. V. Babyr, A. V. Stebnev, V. A. Teremetskaya. Adaptable and energy-effcient powered roof support unit. Mining Informational and Analytical Bulletin. 2022; Vol.6: 46-61. DOI: 10.25018/0236_1493_2022_6_0_46.

[17] L. Yuan. Application of multidirectional robotic wire arc additive manufacturing process for the fabrication of complex metallic parts. IEEE Transactions on Industrial Informatics. 2020; Vol.16: 1-11. DOI: 10.1109/TII.2019.2935233.

[18] F. S. Blaga, A. Pop, V. Hule, and C. I. Indre. The efficiency of modeling and simulation of manufacturing systems using Petri nets. IOP Conference Series: Materials Science and Engineering. 2021; Vol.1169: 012005. DOI: 10.1088/1757-899X/1169/1/012005.

[19] T. Heimig, E. Kerber, S. Stumm, S. Mann, U. Reisgen, and S. Brell-Cokcan. Towards robotic steel construction through adaptive incremental point welding. Construction Robotics. 2020; Vol.4: 49-60. DOI: 10.1007/S41693-019-00026-4.

[20] R. Badarinath and V. Prabhu. Integration and evaluation of robotic fused filament fabrication system. Additive Manufacturing. 2021; Vol. 41: 101951. DOI: 10.1016/J.ADDMA.2021.101951.

[21] S. G. Selivanov, N.K. Krioni, S. N. Poezzhalova. Innovation and innovative design in mechanical engineering: practical work. Ufa: Mashinostroenie; 2013.

[22] S. A. Vasin, A. S. Vasilev, E. V. Plahotkina. Methods for assessing the technical compatibility of heterogeneous elements within a technical system. Journal of Mining Institute. 2020; Vol.243: 329-336. DOI:10.31897/PMI.2020.3.329.

[23] L. Sorrentino. Robotic filament winding: An innovative technology to manufacture complex shape structural parts. Composite Structures. 2019; Vol.220: 699-707. DOI: 10.1016/J.COMPSTRUCT.2019.04.055.

[24] D. Betancur-Vásquez, M. Mejia-Herrera, and J. S. Botero-Valencia. Open source and open hardware mobile robot for developing applications in education and research. HardwareX. 2021; Vol.10: 00217. DOI: 10.1016/J.OHX.2021.E00217.

[25] Y. F. Zhang. Fast-Response, Stiffness-Tunable Soft Actuator by Hybrid Multimaterial 3D Printing. Advanced Functional Materials. 2019; Vol.29: 1806698. DOI: 10.1002/ADFM.201806698.

[26] P. Curkovic and G. Cubric. Fused deposition modelling for 3d printing of soft anthropomorphic actuators. International Journal of Simulation Modelling. 2021; Vol.20: 303-314. DOI: 10.2507/IJSIMM20-2-560.

[27] Yu. D. Vragov. Analysis of the layout of metal-cutting machine tools. Moscow: Mashinostroenie; 1978.

[28] M. Kaur, T. H. Kim, and W. S. Kim. New Frontiers in 3D Structural Sensing Robots. Advanced Materials. 2021; Vol.33: 2002534. DOI: 10.1002/ADMA.202002534.

[29] K. McDonald, A. Rendos, S. Woodman, K. A. Brown, and T. Ranzani. Magnetorheological Fluid-Based Flow Control for Soft Robots. Advanced Intelligent Systems. 2020; Vol.2: 2000139. DOI: 10.1002/AISY.202000139.

[30] K. S. Kulga. Information technologies in the design of mechatronic equipment: textbook. Ufa: UGATU; 2014.

[31] R. Deimel and O. Brock. A novel type of compliant and underactuated robotic hand for dexterous grasping. The International Journal of Robotics Research. 2016; Vol.35: 161-185. DOI: 10.1177/0278364915592961.

[32] E. Thompson-Bean, R. Das, and A. McDaid. Methodology for designing and manufacturing complex biologically inspired soft robotic fluidic actuators: Prosthetic hand case study. Bioinspiration and Biomimetics. 2016; Vol.11: 066005. DOI: 10.1088/1748-3190/11/6/066005.

[33] Y. V. Ilyushin. Development of a Process Control System for the Production of High-Paraffin Oil. Energies. 2022; 15 (17): 6462. DOI: 10.3390/en15176462.

[34] M. T. Bhatti, M. S. J. Hashmi. Software and hardware design of a robotic manipulator for the manufacture of complex shaped dies. Journal of Materials Processing Technology. 1190; Vol.24: 473-493. DOI: 10.1016/0924-0136(90)90208-C.

[35] S. Schiele, H. Phalen, J. Kulozik, Y. S. Krieger, T. C. Lueth. Automated design of underactuated monolithic soft robotics structures with multiple predefined end poses. IEEE International Conference on Robotics and Automation. 2021; Vol.2021-May: 6868-6874. DOI: 10.1109/ICRA48506.2021.9561485.

Civil engineering is an important branch and always making human life safe and cheerfull. Researchers in the field of civil engineering are always enthusistaics and trying to overcome various challenges by providing advance solutions. The scope of civil engineering has widen considerably and it is demand of society to get better solutions through scientific research in various horisons of civil engineering. The better and durable structures, pleasant and healty environment, better transport and automation to assist consturction are some important topics included in this books thorugh six chapters.

GRINREY PUBLISHING

9 788196 410506